https://doi.org/10.5194/essd-2024-420
Preprint. Discussion started: 10 October 2024

Earth System Science Data Discussions
Open Access

Global ocean surface heat fluxes revisited: A new dataset from maximum entropy production framework with heat storage and Bowen ratio optimizations

Yong Yang[1], Huaiwei Sun[1,2,3,4*], Jingfeng Wang[5], Wenxin Zhang[6], Gang Zhao[7], Weiguang Wang[8], Lei Cheng[9], Lu Chen[1], Hui Qin[1], Zhanzhang Cai[6]

[1]School of Civil and Hydraulic Engineering, Huazhong University of Science and Technology, Wuhan 430074, China

[2]Hubei Key Laboratory of Digital River Basin Science and Technology, Huazhong University of Science and Technology, Wuhan 430074, China

[3]Institute of Water Resources and Hydropower, Huazhong University of Science and Technology, Wuhan 430074, China

[4]College of Water Conservancy & Architectural Engineering, Shihezi University

[5.] School of Civil and Environmental Engineering, Georgia Institute of Technology, Atlanta 30318, USA

[6.] Department of Physical Geography and Ecosystem Science, Lund University, Sweden

[7.] Key Laboratory of Water Cycle and Related Land Surface Processes, Institute of Geographic Sciences and Natural Resources Research, Chinese Academy of Sciences, Beijing, China

[8.] College of Hydrology and Water Resources, Hohai University, Nanjing 210098, China

[9.] State Key Laboratory of Water Resources and Hydropower Engineering Science, Wuhan University, Wuhan, China

Correspondence to: Huaiwei Sun (hsun@hust.edu.cn) and Wenxin Zhang (wenxin.zhang@nateko.lu.se)

Abstract. Ocean evaporation (latent heat flux, LE) plays a crucial role in global precipitation patterns, water cycle dynamics, and energy exchange processes. However, current bulk methods for quantifying ocean evaporation are subject to significant uncertainties. The Maximum Entropy Production (MEP) theory offers a novel approach for estimating surface heat fluxes, but its effectiveness over ocean surfaces has not been validated. This study integrates heat storage effects and four empirical Bowen ratio formulas into the MEP theory to improve ocean LE estimation. We employed multi-source data from 129 globally distributed buoy stations and seven auxiliary turbulent flux datasets for validation and comparison. We first evaluated the MEP method using observed data from buoy stations, identifying the optimal Bowen ratio formula to enhance the model. Results indicate that accounting for heat storage and adjusting the Bowen ratio significantly improve heat flux accuracy, with R^2=0.99 and a root mean squared error (RMSE) of 4.7 $W \cdot m^{-2}$ compared to observations. Subsequently, we conducted a thorough evaluation of seven global turbulent flux datasets to identify the most accurate input variables (e.g., heat storage, net radiation, surface temperature) for applying the MEP method on a global ocean scale. The enhanced MEP method provided new estimates of the annual

https://doi.org/10.5194/essd-2024-420
Preprint. Discussion started: 10 October 2024

Open Access Earth System Science Data Discussions

average LE at 93 W·m^{-2} and sensible heat at 12 W·m^{-2} for the period 1988 to 2017. Validation against observations from 129 buoy stations demonstrated that the MEP-derived latent heat dataset achieved the highest accuracy, with a mean error (ME) of 1.3 W·m^{-2}, an RMSE of 15.9 W·m^{-2}, and a Kling-Gupta Efficiency (KGE) of 0.89, outperforming four major long-term global heat flux datasets, including J-OFURO3, ERA5, MERRA2, and OAFlux. Additionally, we examined the long-term spatiotemporal variability of global ocean evaporation, identifying a significant increasing trend from 1988 to 2010 at a rate of 3.58 mm/yr, followed by a decline at a rate of -2.18 mm/yr from 2010 to 2017. The current dataset provides a new benchmark for the ocean surface energy budget and is expected to be valuable for research on global ocean warming, sea surface-atmosphere energy exchange, the water cycle and climate change. The monthly MEP heat flux dataset for 1988–2017 is publicly available at https://doi.org/10.6084/m9.figshare.26861767.v2 (Yang et al., 2024, last access: 28 August 2024).

1. Introduction

The ocean system plays a pivotal role in regulating the global climate by receiving and redistributing heat and freshwater, thereby influencing Earth's energy balance and the dynamics of the water cycle (Li et al., 2023; Von Schuckmann et al., 2023; Marti et al., 2022; Johnson et al., 2020). A key component of this regulation is ocean evaporation (latent heat), which accounts for approximately 86% of atmospheric water vapor and is the primary driver of the global hydrological cycle (Yu, 2011). As climate change warms the ocean, evaporation rates are anticipated to rise, potentially intensifying the global hydrological cycle (Masson-Delmotte et al., 2021). This intensification could alter precipitation patterns, affecting regional water availability and freshwater ecosystems (Konapala et al., 2020; Roderick et al., 2014). Therefore, precise estimation of ocean evaporation is critical to understand and quantify the global energy and water budget (Iwasaki et al., 2014).

Current methods for calculating surface latent heat (*LE*) and sensible heat flux (*H*) employ bulk transfer formulations that necessitate extensive parameterization inputs, including temperature gradients, humidity gradients, wind speed, and transfer coefficients (Fairall et al., 1996; Andreas et al., 2008). Despite their widespread application, these bulk methods encounter significant limitations primarily due to challenges in accurately parameterizing and empirically deriving coefficients (Zeng et al., 1998; Robertson et al., 2020). These methods heavily depend on assumptions regarding atmospheric stability and boundary layer dynamics, which may not consistently apply across diverse and complex environmental conditions (Fairall et al., 2003; Andreas et al., 2013). Furthermore, uncertainties in estimating turbulent transfer coefficients can lead to substantial errors in the estimation of latent heat flux. The high demands for parameterization and challenges in data acquisition contribute to considerable uncertainties when implementing bulk methods for calculations. While numerous energy balance-based algorithms have been developed to estimate global terrestrial evapotranspiration (Wang et al., 2012; Yang et al., 2023), similar efforts to apply these algorithms for estimating ocean surface heat flux remain unexplored. Therefore, proposing an innovative method for estimating ocean surface heat flux based on rational surface energy allocation could yield significant theoretical and practical implications. This approach may serve as an additional reference source for existing bulk methods and their derived datasets, offering a new methodological perspective for quantifying the uncertainty of ocean heat flux estimation. Ultimately, this could facilitate more accurate ocean flux estimation and enhance research on ocean energy allocation patterns.

The Maximum Entropy Production (MEP) model, an energy-balance-based approach, has recently emerged as a novel method for simulating surface heat fluxes. Developed from Bayesian probability theory and information theory, it prioritizes the most probable partitioning of radiation fluxes (Wang & Bras, 2011). The MEP model has been rigorously validated across diverse surface types and varying degrees of surface wetness (Wang et al., 2014; Huang et al., 2017; Yang et al., 2022; Sun et al., 2022; Sun et al., 2023). Notably, the MEP model requires fewer input variables—net radiation, surface temperature, and specific humidity—yet provides accurate estimates of latent heat, sensible heat, and ground heat fluxes simultaneously. Unlike bulk methods (Fairall et al., 2003), which rely on wind speed, temperature gradient, and humidity gradient, the MEP model satisfies the energy balance constraint without these dependencies. This characteristic enhances its applicability and robustness across diverse environmental conditions. However, the previous application of the MEP model over ocean surfaces has revealed significant limitations, including notable underestimations of latent heat and overestimations of sensible heat flux (Huang et al., 2017). The global multi-year averaged *LE* estimated by the MEP model indicates a value around 58 W·m^{-2}, much lower than the range of 92~109 W·m^{-2} reported by other remote sensing or reanalysis-based products. Conversely, MEP estimates an averaged *H* of approximately 28 W·m^{-2}, which is significantly higher compared to values ranging from 6 to 18 W·m^{-2} found in other products. These discrepancies highlight substantial uncertainties in applying the MEP model to oceanic energy partitioning, highlighting the urgent need for further refinement and rigorous validation efforts.

https://doi.org/10.5194/essd-2024-420
Preprint. Discussion started: 10 October 2024

The Bowen ratio (B_o), defined as the ratio of sensible heat to latent heat flux ($B_o = H/LE$), is crucial for understanding the energy partitioning process (Hicks & Hess, 1977). In the context of the energy balance-based MEP model, the significant overestimation of B_o suggests that focusing on this ratio can enhance our understanding of energy partitioning dynamics (Andreas et al., 1996). Studies have highlighted that the actual Bowen ratio over ocean surfaces (B_{oa}) often diverges from the equilibrium Bowen ratio (B_o^*) observed under ideal conditions where the air is saturated with water vapor. The B_{oa} may deviate significantly from B_o^* under non-equilibrium conditions, which are typical in most environments (Jo et al., 2002; Andreas et al., 2013), posing challenges in establishing a robust relationship between B_{oa} and B_o^* (Liu & Yang, 2021). Therefore, developing an accurate $B_o^* \sim B_{oa}$ relationship is crucial for refining the energy partitioning process in the MEP model. The advancement of buoy observation networks has provided compelling evidence for validating ocean heat fluxes and has become crucial in assessing their associated uncertainties (Bourras, 2006; Smith et al., 2011; Bentamy et al., 2017; Liang et al., 2022; Tang et al., 2023). This study utilizes the energy balance-based MEP method to estimate ocean evaporation, introducing a novel approach to redistributing surface energy budgets and offering a streamlined parameterization scheme distinct from conventional bulk methods used for estimating ocean heat fluxes. In contrast to existing approaches that using reanalysis-based schemes (e.g., NCEP, ECMWF, and GEOS) and their associated parameterizations (Tang et al., 2024) to estimate LE, this study employs satellite observations to directly estimate ocean heat fluxes, thereby minimizing error propagation associated with the model structures and assimilation schemes.

The primary objectives of this study are as follows: (1) to develop and validate the MEP approach for estimating ocean heat fluxes using observations from 129 stations; (2) to investigate the impact of heat storage on ocean energy allocation and the influence of the Bowen ratio on energy partitioning for heat flux estimations; (3) to produce a MEP-derived ocean heat fluxes product (spatial resolution: 0.25°; temporal coverage: 1988-2017) and present its spatiotemporal patterns.

2. Methods

2.1 Components of ocean surface energy balance

The global ocean energy balance equation is as follows (Meehl, 1984; Wang et al., 2021):

$$R_n = LE + H + G \tag{1}$$

https://doi.org/10.5194/essd-2024-420
Preprint. Discussion started: 10 October 2024

$$R_n = R_{ns} + R_{nl} = R_s^{\downarrow} - R_s^{\uparrow} + R_l^{\downarrow} - R_l^{\uparrow} \tag{2}$$

where R_n, R_{ns}, R_{nl} are net radiation, net shortwave radiation (the difference of incoming radiation $R_s^{\downarrow}$ and reflected solar radiation $R_s^{\uparrow}$), and net longwave radiation (the difference of incoming longwave radiation $R_l^{\downarrow}$ and outgoing longwave radiation $R_l^{\uparrow}$), H is sensible heat, LE is latent heat, and G is the heat flow through the surface. Unlike terrestrial surfaces, the energy balance equation for the ocean surface accounts for distinct energy exchange processes, including the impact of seawater mixing and dynamics on energy transfer. For the ocean surface, the flux term G has two components,

$$G = \mathrm{G}_t + G_v \tag{3}$$

where G_t is the change in the ocean heat content (ΔOHC, or heat storage), and G_v is the lateral heat transported by ocean currents and other processes. The G_t can be quantified as the vertical integration of temperature profile in a column of depth (Meehl ,1984, Li et al., 2023). Both the heat storage and the ocean heat transport G_v are difficult to quantify, which requires large masses of hydrographic variables and performing integrations at different depths. Since the previous study overlooked the calculation of evaporation on a global scale (Wang et al., 2021), leading to the G flux being equal to heat storage. For the convenience in description, this study will consider the concept of G flux as equivalent to heat storage.

2.2 The Maximum Entropy Production theory

2.2.1 The original MEP model

The MEP model simulate ocean surface heat fluxes using inputs variables of net radiation (R_n), surface skin temperature (T_s), and surface specific humidity (q_s) under the constraint of the surface energy balance. The latent heat, sensible heat, and surface thermal energy flux (Q) are calculated as,

$$[1 + B(\sigma) + \frac{B(\sigma)}{\sigma}\frac{I_s}{I_0}|H|^{-\frac{1}{6}}]H = R_n \tag{4}$$

$$E = B(\sigma)H \tag{5}$$

$$Q = R_{nl} - E - H \tag{6}$$

$$B(\sigma)=6(\sqrt{1+\frac{11}{36}\sigma}-1),\quad \sigma=\frac{\lambda^2}{c_p R_v}\frac{q_s}{T_s^2} \tag{7}$$

$$I_0=\rho_a c_p\sqrt{C_1 kz}(C_2\frac{kzg}{\rho_a c_p T_r})^{\frac{1}{6}} \tag{8}$$

where $B(\sigma)$ is the reciprocal Bowen ratio, σ is a dimensionless parameter that characterizes the phase change at the ocean surface, λ (J·kg^{-1}) is the latent heat of vaporization of liquid surface, c_p (10^3 J·kg^{-1}·K^{-1}) is the specific heat of air under constant pressure, and R_v (461 J·kg^{-1}·K^{-1}) is the gas constant of water vapor. I_0 is the "apparent thermal inertia" of air and describes the turbulent transport process of the boundary layer based on the Monin-Obukhov similarity theory (MOST) (Wang and Bras, 2010). I_s is the thermal inertia of the ocean surface (J·m^{-2}·K^{-1}·s$^{-1/2}$), and can be parametrized as $I_s=\sqrt{\rho c\lambda}$ (with density ρ, the specific heat c) represents the physical property of surface (I_s=1.56×10^3 J·m^{-2}·K^{-1}·s$^{-1/2}$ for water surface and 1.92×10^3 J·m^{-2}·K^{-1}·s$^{-1/2}$ for ice surface) .

Over the sea ice surface, assumed to be saturated, the specific humidity q_s can be derived as a function of surface temperature T_s using the Clausius-Clapeyron equation. (El Sharif et al., 2019; Shaman & Kohn, 2009).

$$q_s=\varepsilon\frac{e_s(T_s)}{P}=\varepsilon\frac{e_0}{P}\exp[\frac{\lambda_s}{R_v}(\frac{1}{T_0}-\frac{1}{T_s})] \tag{9}$$

where ε (= 0.622) represents the ratio of the molecular weight of water vapor to that of dry air, $e_s(T_s)$ denotes the saturation vapor pressure at temperature Ts, e_0 is the saturation vapor pressure at the reference temperature T_0 (273.15 K), and P is the atmospheric pressure (mb).

2.2.2 Specific improvements on the MEP model

Equations (4) ~ (9) presented above represent the original formulas of the MEP model. According to the MEP theory, the net solar radiation (R_{ns}) entering the water surface medium is absorbed by the water body, with the allocable radiation flux denoted as $R_{nl}=E+H+Q$ (Eq.6). Consequently, the expression for

https://doi.org/10.5194/essd-2024-420
Preprint. Discussion started: 10 October 2024

ocean heat uptake (heat storage) is derived as $G = R_n - E - H = R_{ns} + Q$. While this theory has received preliminary validation in shallower water bodies, such as lake surfaces (Wang et al., 2014), its applicability on deeper water bodies with larger heat storage capacities in ocean surfaces requires further evaluation. This study introduces two key hypotheses: (1) The substantial heat storage capacity of the ocean can exert a significant influence on seasonal latent and sensible fluxes, potentially introducing bias to the MEP equations, (2) The notable underestimation of latent heat flux and overestimation of sensible heat flux by the MEP model point to a significant deviation from the Bowen's ratio formula, necessitating a reasonable correction. To address this, the study proposes two approaches for enhancing the MEP formulas: (1) Considering the impact of heat storage in the MEP's energy balance equation, and (2) Adjusting the theoretical equilibrium Bowen ratio within the MEP model. This can be specifically represented as follows:

$$[1+\frac{1}{B_o^*}]H = R_n - G \tag{10}$$

$$B_o^* = \frac{1}{B(\sigma)} \tag{11}$$

$$B_{oa} = a \times B_o^* + b \tag{12}$$

where B_o^* is the equilibrium Bowen ratio, which denotes the theoretical ratio of sensible heat flux to latent heat flux when the surface and the atmosphere are in equilibrium regarding water vapor. Correspondingly, the corresponding evaporation at this condition is known as equilibrium evaporation (defined as the water vapor evaporating from a saturated surface into a saturated atmosphere). To accurately predict actual evaporation, a reliable functional relationship needs to be established to predict B_{oa} from B_o^*. Empirical studies have introduced coefficients to correlate B_o^* to B_{oa} under diverse environmental circumstances; for instance, the Priestley–Taylor coefficient is expressed as (Priestley & Taylor, 1972).

$$B_{oa} = 0.79 \times B_o^* - 0.21 = \frac{0.79 - 0.21 \times B(\sigma)}{B(\sigma)} \tag{13}$$

Further studies have led to the emergence of more updated empirical coefficients. Hicks and Hess (1977) estimated the actual Bowen ratio as $B_{oa} = 0.63 \times B_o^* - 0.15$ by aligning it with direct observations of the fluxes. Yang & Roderick (2019) deduced an empirical coefficient of 0.24 and formulated it as

https://doi.org/10.5194/essd-2024-420
Preprint. Discussion started: 10 October 2024

$B_{oa} = 0.24 \times B_o^*$ through fitting Bowen ratio and surface temperature data across the global ocean surface. Furthermore, Liu & Yang (2021) derived a new equation as $B_{oa} = 0.37 \times B_o^* - 0.05$ based on the atmospheric boundary layer model. Given their favorable spatial applicability and representativeness, this study opted to utilize these four $B_{oa} \sim B_o^*$ formulas to refine the MEP model and assess their suitability. The revised reciprocal actual Bowen ratio is represented as,

$$\begin{cases} B(\sigma)_{a1} = \dfrac{1}{B_{oa}} = \dfrac{B(\sigma)}{0.79 - 0.21 \times B(\sigma)} \\ B(\sigma)_{a2} = \dfrac{1}{B_{oa}} = \dfrac{B(\sigma)}{0.63 - 0.15 \times B(\sigma)} \\ B(\sigma)_{a3} = \dfrac{1}{B_{oa}} = \dfrac{B(\sigma)}{0.24} \\ B(\sigma)_{a4} = \dfrac{1}{B_{oa}} = \dfrac{B(\sigma)}{0.37 - 0.05 \times B(\sigma)} \end{cases} \tag{14}$$

where $B(\sigma)_{a1} \sim B(\sigma)_{a4}$ represent the four empirical Bowen ratio formulas for comparisons in this study. Thus, the improved MEP model is complemented as: replacing the original $B(\sigma)$ with the corrected $B(\sigma)_a$, then combining Eq. (5), (7)-(9), and (14) into the MEP energy balance equation considering heat storage (Eq. (10)), ultimately leading to the determination of latent and sensible heat flux.

2.3 Input data for MEP model

The performance of both the original and improved Maximum Entropy Production (MEP) models is evaluated using observed data from in-situ buoy stations, as discussed in Section 3.1. Subsequently, the optimal empirical Bowen ratio formula for the MEP model is determined through multi-site assessments. The refined MEP model is then applied to estimate global heat fluxes based on long-term remote-sensing observations, detailed in Sections 3.2 and 3.3, following a comprehensive evaluation of input parameters. Specifically, the input variables of net radiation, heat storage, and sea surface temperature driving the improved MEP model are derived from the J-OFURO3 dataset, covering the period from 1988 to 2017 at a spatial resolution of 0.25° (detailed in Section 4.3).

https://doi.org/10.5194/essd-2024-420
Preprint. Discussion started: 10 October 2024

2.4 Sensitivity analysis

To quantify the influence of input variables in the MEP model on evaporation estimate at the ocean surface, sensitivity coefficients (S) are computed as (Beven, 1979; Isabelle et al., 2021),

$$S_i = \frac{\partial LE}{\partial x_i}\frac{x_i}{LE} \quad (15)$$

where S_i represents the sensitivity coefficient of *LE* to each variable x_i. The magnitude of S_i reflects the degree of impact of the variable's changes on LE; a larger absolute value indicates a greater influence of the variable on *LE*. A positive value signifies a positive correlation between evaporation and the variable's changes, while a negative value indicates a negative correlation. For example, a sensitivity coefficient of 0.5 represents that a 10% increase in the variable would result in a 5% increase in *LE*. The sensitivity levels can be categorized based on the absolute value |Si| (Lenhart et al., 2002; Yin et al., 2010): |Si| > 1 indicates very high sensitivity, 1 > |Si| > 0.2 denotes high sensitivity, 0.2 > |Si| > 0.05 reflects moderate sensitivity, and |Si| < 0.05 suggests negligible sensitivity.

2.5 Data fusion methods

To identify the globally optimal heat storage input data (refer to Section 4.3), this study attempts to determine whether data fusion methods could yield results superior to individual datasets. This includes the Bayesian Three-Cornered Hat (BTCH) Method (He et al., 2020) and the Simple Arithmetic Average (AA) method. The Three-Cornered Hat (TCH) method has been widely applied to improve accuracy by integrating multi-source products, and it has been proven to outperform individual parent products (Long et al., 2017; Liu et al., 2021; Duan et al., 2024). Recent evaluations of three distinct data fusion methods (TCH, BTCH, and AA) in consolidating evapotranspiration estimates have affirmed their efficacy in filtering poor ET products, but their ability to reliably identify superior ET products remains uncertain (Shao et al., 2022). For instance, the AA method may yield better results than the BTCH method in some instances. Consequently, following a comparative analysis of the accuracy of individual, BTCH, and AA fusion products, this study selects the optimal heat storage dataset to drive the MEP model. Since BTCH is not the primary focus of this study, detailed method descriptions are referred to He et al. (2020).

https://doi.org/10.5194/essd-2024-420
Preprint. Discussion started: 10 October 2024

3. Data materials

3.1 In situ buoy observations

A total of 129 in situ buoy sites were employed for ocean heat fluxes calculation and validation with MEP model and its modified version, as listed in Table 1. About 96% of selected sites (124 of 129 all sites) are collected from the Global Tropical Moored Buoy Array (available at https://www.pmel.noaa.gov/), which consists of the TAO/TRION Pacific Ocean (69 buoys), PIRATA Atlantic Ocean (23 buoys), and RAMA Indian ocean (32 buoys), and the remaining sites including Upper Ocean Processes Group (3 buoys) consists of Project WHOTS - WHOI Hawaii Ocean Time-series Station (available at https://uop.whoi.edu/ReferenceDataSets/whotsreference.html), Project NTAS - Northwest Tropical Atlantic Station and Project STRATUS (https://uop.whoi.edu/ReferenceDataSets/ntasreference.html), and the Pacific ocean climate stations (2 buoys) consists of KEO and PAPA moorings (https://www.pmel.noaa.gov/ocs/data/fluxdisdel/). The availability of all buoy stations refers to the "Data availability" section. The observational sites cover the spatial range of 25°S~ 50.1°N latitude, temporal range span from 1989/12 to 2023/12. Observational meteorological variables and heat fluxes includes the net longwave radiation, net shortwave radiation, sea surface skin temperature, specific humidity at 2m height (if available, or computed as the function of SST according to the Clausius-Clapeyron equation), latent heat flux and sensible heat flux. Limited by the availability of longwave radiation observations, the net radiation has a relatively shorter time series length compared to latent and sensible heat fluxes. The surface air-sea fluxes of buoy observations are computed using the COARE 3.0b algorithm, which have been widely applied for fluxes estimations and validations (Tang et al., 2023; Bentamy et al., 2017; Fairall et al., 2003). All the selected original buoy observation (except for KEO and Papa sites) records are in monthly temporal resolution, and the original daily observations of KEO and Papa has been aggregated to monthly by simple average method. The spatially distributed map of all selected sites is illustrated in Fig.S1.

Table 1. Information about observational ocean surface heat fluxes of 129 buoy sites

Buoy array	Buoy amount	Spatial coverage	Temporal coverage	Number of *LE* (*H*) records	Number of R_n records
TAO/TRION pacific	69	165°E-95°W 10°S-10°N	1989/12/16-2023/12/16	12377	522

https://doi.org/10.5194/essd-2024-420
Preprint. Discussion started: 10 October 2024

PIRATA Atlantic	23	40°W-10°E, 20°S-20°N	1997/9/16-2023/12/16	2644	631
RAMA Indian	32	55°E-100°E, 25°S-15°N	2001/11/16-2023/12/16	1862	286
WHOTS	1	158°W, 22.7°N	2004/08/15-2021/08/15	205	205
NTAS	1	51°W, 15°N	2001-04/15-2020/03/15	219	219
STRATUS	1	85.4°W, 19.6°S	2000/10/15-2021/01/15	235	235
KEO	1	144.6°E, 32.3°N	2004/06/17-2023/08/12	177	177
PAPA	1	144.9°W, 50.1°N	2007/06/08-2023/11/14	181	181

Note: The number of records represents the effective count (excluding NA values) of latent and sensible heat flux observations.

3.2 Global turbulent heat flux datasets for evaluations

This study evaluates and compares 7 global turbulent heat flux products with observations, categorizing them into three types: Remote sensing-based, atmosphere reanalysis-based, and hybrid-based (Table 2). These seven products encompass monthly data spanning from 1988 to 2017, with spatial resolutions ranging from 0.25° to 1°. The criterion for dataset filtering prioritizes products that feature relatively longer time series, typically exceeding 15 years.

The Clouds and Earth's Radiant Energy Systems Synoptic Edition 4A (CERES SYN1deg_Ed4A, hereafter referred to as CERES4, available at https://ceres.larc.nasa.gov/data/) offers net radiation data, derived from clear-sky upward shortwave, downward shortwave flux, upward longwave, and downward longwave flux measurements (Wielicki et al., 1996; Rutan et al., 2015). Another remote sensing-based radiation product, the Global Energy and Water Cycle Experiment - Surface Radiation Budget (GEWEX-SRB, available at https://asdc.larc.nasa.gov/project/SRB) (Pinker et al., 1992), in conjunction with CERES4, demonstrates good accuracy in retrieving R_n, as validated by six global observing networks (Liang et al., 2022).

The J-OFURO3 is the third-generation dataset developed by the Japanese Ocean Flux Data Sets with use of the Remote-Sensing Observations (J-OFURO) research project (available at https://j-ofuro.isee.nagoya-u.ac.jp/en/) (Tomita et al., 2019). It calculates turbulent heat flux with the latest version of

https://doi.org/10.5194/essd-2024-420
Preprint. Discussion started: 10 October 2024

COARE3.0 algorithm, and provides datasets for R_n, *LE*, *H* and *SST* in this study. Validation with in situ observations showed that J-OFURO3 offered a superior performance of latent heat compared to other 5 satellite products from 2002-2013 (Tomita et al., 2019).

Two Atmosphere reanalysis products including the fifth generation European Centre for Medium-Range Weather Forecasts (ECMWF) atmospheric Re-Analysis52 (ERA5, available at https://cds.climate.copernicus.eu/cdsapp#!/dataset/reanalysis-era5-single-levels-monthly-means?tab=overview) (Hersbach et al., 2020), and the Modern-Era Retrospective analysis for Research and Applications Version2 (MERRA2, available at https://disc.gsfc.nasa.gov/datasets/M2TMNXOCN_5.12.4/summary) (Gelaro et al., 2017). Both ERA5 and MERRA2 products employ the bulk formula based on the MOST to calculate heat fluxes. Validation results from previous studies have demonstrated good consistency with buoy estimates regarding heat fluxes (Pokhrel et al., 2020; Chen et al., 2020).

The OAFlux (available at https://oaflux.whoi.edu/), a hybrid-based product developed under the Objectively Analyzed Air-Sea Fluxes (OAFlux) project at the Woods Hole Oceanographic Institution (WHOI) (Yu et al., 2008), was utilized for comparisons with ocean heat fluxes derived from distinct methods. This product calculates fluxes based on the COARE3.0 bulk algorithm and employs a variational objective analysis to determine the optimal fitting of independent variables. Detailed descriptions on all utilized global turbulent heat fluxes products, and their validation performances against buoy observations with reported studies are available in Tang et al (2023).

Table 2. The information of the 7 used global radiation and heat fluxes products

Product	Variables	Spatial resolution	Time span	Type	Reference
CERES4	R_n	1°	2000-2017	Remote sensing	Rutan et al. (2015)
GEWEX-SRB	R_n	1°	1988-2017	Remote sensing	Pinker et al. (1992)
J-OFURO3	R_n, *SST*, *LE*, *H*	0.25°	1988-2017	Remote sensing	Tomita et al. (2019)
ERA5	R_n, *LE*, *H*, *P*	0.25°	1988-2017	Atmosphere reanalysis	Hersbach. et al. (2020)

https://doi.org/10.5194/essd-2024-420
Preprint. Discussion started: 10 October 2024

MERRA2	R_n, *LE*, *H*	1/2° × 2/3°	1988-2017	Atmosphere reanalysis	Gelaro et al. (2017)
OAFlux	*LE*, *H*	1°	1988-2017	Hybrid-based	Yu et al. (2008)
IAPv4-OHC	*OHC*	1°	1988-2017	Hybrid-based	Cheng et al. (2017)

https://doi.org/10.5194/essd-2024-420
Preprint. Discussion started: 10 October 2024

3.3 Ocean heat content data

Remote sensing data for heat storage (G) primarily derive from two categories: one is obtained from the residual of the energy balance equation (R_n-LE-H), including J-OFURO3, ERA5, and MERRA2; the other is calculated as changes in Ocean Heat Content (OHC). The ocean heat content data is obtained from IAP OHC gridded analysis (IAPv4, available at http://www.ocean.iap.ac.cn/) dataset, covering ocean depth of 0-6000m (Cheng et al., 2017), and has been extensively utilized in global ocean heat analysis, ocean warming, and climate change studies (Li et al., 2023; Cheng et al., 2022; Cheng et al., 2024). The delta OHC is calculated using the numerical differentiation method (Xu et al., 2019) as $\Delta \mathrm{OHC(i)} = \frac{OHC(i+1)-OHC(i-1)}{2\Delta i}$, i denotes the OHC of i-th month. At the WHOTS site, this study compared the OHC changes at different depths with the observed G (derived as Rn-LE-H) (Fig.S1). Since the OHC variation from 0~100m depth exhibits the smallest error with the observations, the data from 0~100m depth range were chosen as the heat storage. This study assesses the suitability of G flux and $\Delta \mathrm{OHC}$ for global evaporation estimations, with the aim of minimizing the errors introduced by input variable data in the MEP model.

This study evaluates the accuracy of all the variables R_n, T_s, and G using the aforementioned datasets on a global scale by comparing them against buoy observations (in Section 4.3), to optimize input accuracy for driving the MEP model. To maintain consistency in the analysis, this study resamples all products to a 1° spatial resolution when comparing the Bowen ratio across multiple products. Nevertheless, when conducting site validations with buoy observations, the original resolution of the data is preserved to minimize uncertainty attributable to scale effects.

4. Results

4.1 The new MEP model with heat storage and the revised Bowen ratio formulas

To demonstrate how the MEP model has been developed and improved, we show the comparisons of different MEP models in simulating heat fluxes across 129 global buoy stations (Fig.1). Limited by the availability of R_{nL} data, we used $LE + H$ instead of the available energy ($R_n - G$), enabling the utilization of more observational records to verify the MEP model. The original MEP model (without considering heat

https://doi.org/10.5194/essd-2024-420
Preprint. Discussion started: 10 October 2024

storage) shows a significant negative correlation between *LE* and *H* (with R^2 exceeds 0.65 as in Fig.1a & Fig.1c), with considerable errors, where the RMSE of *LE* is 134.6 $W \cdot m^{-2}$ and that of *H* is 37 $W \cdot m^{-2}$. Upon modification by considering the influence of heat storage effects (Represented as *MEP_M*, as depicted in Fig.1b & Fig.1h), the MEP-simulated *LE* shows a good consistency ($R^2 = 0.97$) with the buoy observations, but an approximate 25% underestimation (slope = 0.75) was observed, with RMSE reduced to 27 $W \cdot m^{-2}$. However, it reveals an overall underestimation (approximate 25%) of *LE* and a large overestimation of *H*. This finding agrees with previous research findings that equilibrium evaporation tends to underestimate actual evaporation from saturated surfaces by 20%~30% (Yang & Roderick, 2019; Philip, 1987). The physical significance of this phenomenon can be explained as the equilibrium evaporation being considered the lower limit of actual evaporation from saturated surfaces, causing typically falls below the actual evaporation (Priestley and Taylor, 1972). To address the deviation between B_{oa} and B_o^*, it is necessary to convert the equilibrium Bowen ratio into the actual Bowen ratio, allowing for a more reasonable and accurate allocation of surface energy budget.

After modifying MEP's energy allocation using four empirical Bowen ratio formulas (denoted as *M_0.24*, *M_0.79*, *M_0.63*, *M_0.37*), the accuracy of MEP predated latent and sensible heat have been significantly improved. The MEP simulated *LE* exhibited strong agreement with observations, with all R^2 exceeding 0.97 and RMSE ranging from 4.7 $W \cdot m^{-2}$ (for *M_0.24*) to 7.1 $W \cdot m^{-2}$ (for *M_0.79*), which is lower than that derived from equilibrium Bowen ratios (RMSE = 27 $W \cdot m^{-2}$). Both *M_0.79* and *M_0.63* tended to underestimate *LE*, especially when *LE* exceeded 200 $W \cdot m^{-2}$ (Fig. 1d and Fig.1e). The results for sensible heat flux simulated by MEP were similar to those for *LE*, the *M_0.24* outperformed the other three, showing the smallest errors and highest R^2.

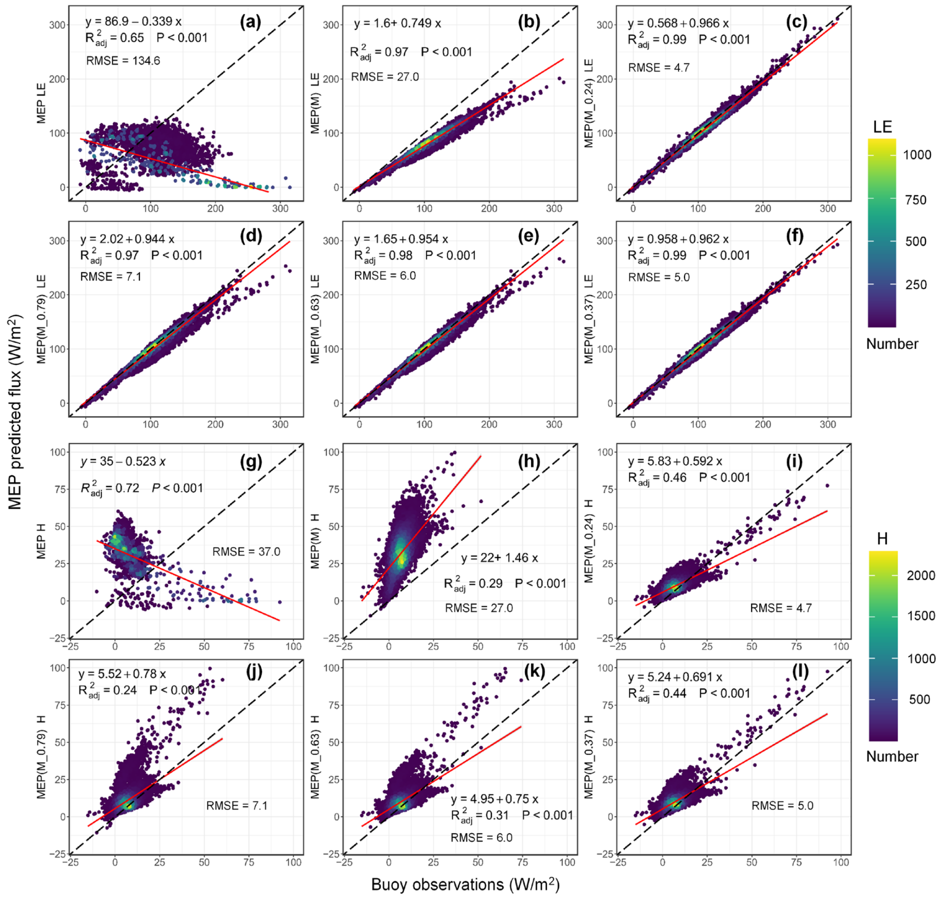

Figure 1. Scatter density plots of monthly latent heat flux (a~f) and sensible heat flux (g~l) derived by the original and modified MEP methods versus observations from 129 buoy stations (as in Table 1). (a) The original MEP method, (b) The modified MEP method considering the heat storage effect, (c) The modified MEP method considering both the heat storage and empirical Bowen ratio formula $B_{oa}=0.24B_o^*$, (d)~(f) for the modified MEP method considering both the heat storage and empirical Bowen ratio formulas B_{oa}=0.79B_o^*-0.21, B_{oa}=0.63B_o^*-0.15, and B_{oa}=0.37B_o^*-0.05. (g)~(l) are the same with (a)~(f) but for sensible heat flux.

Specifically, the spatial errors for the four modified MEP formulas were obtained (Fig. 2), as well as the prediction errors across various observational buoy arrays (Fig.3). Overall, the four modified MEP formulas exhibit lower errors at low latitudes (10°S~10°N), but they demonstrate larger discrepancies at higher latitudes, especially for the KEO, WHOTS, and STRATUS buoy sites. Comparing the four formulas across varying latitudes, the *M_0.24* formula exhibits the smallest RMSE (ranging from 3.6 to 12 W·m^{-2}) (Fig. 3c), while the *M_0.79* formula shows the largest errors (RMSE ranging from 3.9 to 26.6 W·m^{-2}). This consistency

https://doi.org/10.5194/essd-2024-420
Preprint. Discussion started: 10 October 2024

is also evident in the Kling-Gupta Efficiency (KGE) coefficient, with *M_0.24* demonstrating superior performance in terms of accuracy, robustness, and adaptability. In term of *M_0.24* formula, the prediction errors across observational arrays ranked as: RAMA < PIRATA < TAO/TRION < PaPa < KEO < STRATUS < WHOTS < NTAS. The arrays with relatively larger RMSE (NTAS in the Atlantic Ocean, WHOTS, and STRATUS in the Pacific Ocean) may originate from the larger observed values of LE (Fig. S2).

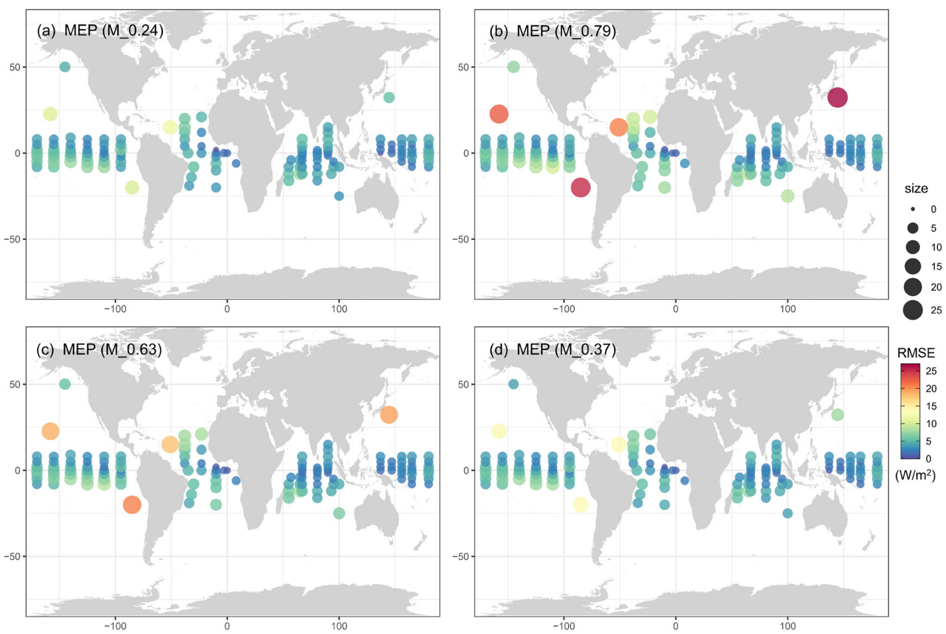

Figure 2. Spatial distribution of RMSE values in the comparison of latent heat flux estimated by the improved MEP method (modified by four different Bowen ratio formulas) with buoy observations from 129 stations.

https://doi.org/10.5194/essd-2024-420
Preprint. Discussion started: 10 October 2024

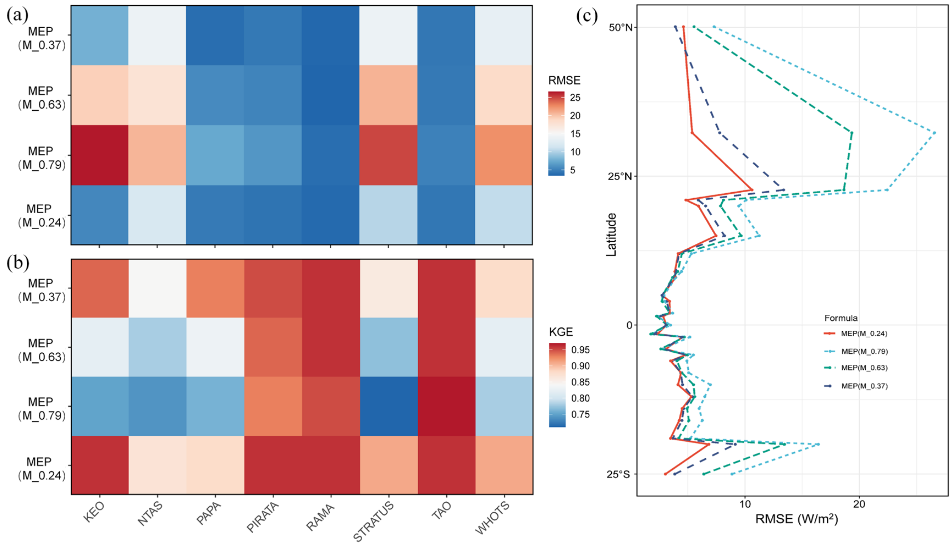

Figure 3. Comparisons of latent heat flux estimated by the improved MEP method with buoy observations from each buoy array in term of RMSE (a) KGE value (b), and latitudinal means of RMSE of four empirical Bowen ratio formulas (c). Latitudinal means are based on data from 129 available buoy sites.

4.2 Dynamics of heat fluxes and Bowen ratio between original and improved MEP model

To thoroughly investigate the role of heat storage in the partitioning of surface energy and its implications for the temporal dynamics of heat fluxes, we selected the KEO site for detailed analysis. This decision was based on the site's extensive long-term observational records and notable variability in flux patterns, which offer an ideal context for a rigorous comparison of model-simulated error margins.

The improved MEP methods demonstrated comparable performance in estimating heat fluxes at the KEO site when compared with 128 other sites (Fig. S3, Fig. 1), with the MEP (M_0.24) model exhibited the most effective performance. Analysis of the time series data revealed significant variations in latent heat, sensible heat, and Bowen ratio (Fig. 4). In the original MEP theory, the estimated *LE* exhibits an opposite variation cycle (peak versus trough) compared to the observations. For instance, over a yearly period, the observed peak in *LE* occurred in January 2005 (269 $W \cdot m^{-2}$) and the trough in June 2005 (6.9 $W \cdot m^{-2}$). In contrast, the MEP simulated the peak in *LE* to occur in August 2005 (105 $W \cdot m^{-2}$) and the trough in December 2004 (0.7 $W \cdot m^{-2}$), resulting in a phase difference of 7 months for the peak and 6 months for the trough values. Sensible heat flux (Fig. 4b) showed similar phase differences: observed *H* peaked in January 2005 (79 W·m⁻

https://doi.org/10.5194/essd-2024-420
Preprint. Discussion started: 10 October 2024

^{2}) and reached its minimum in June 2005 (-3 W·m^{-2}), whereas MEP simulated H to peak in August 2005 (46 W·m^{-2}) and reach its minimum in December 2004 (0.6 W·m^{-2}), consistent with the pattern observed for LE. It is noteworthy that the original MEP model simulated variations in LE and H align with R_n (Fig. S4), which is reasonable over land where the small G value can often be disregarded. However, over the ocean, the observed variations in R_n and LE do not align in terms of their cycles. The maximum R_n occurred in June 2004 (329 W·m^{-2}) and the minimum occurred in December 2004 (142 W·m^{-2}), with a 6-month delay in relation to the variations in LE. Specifically, the peak R_n corresponded to the trough of LE, and the trough R_n corresponded to the peak of LE. This delay indicates that the heat storage effect delays the peak of LE and alters the seasonal variations of LE and H.

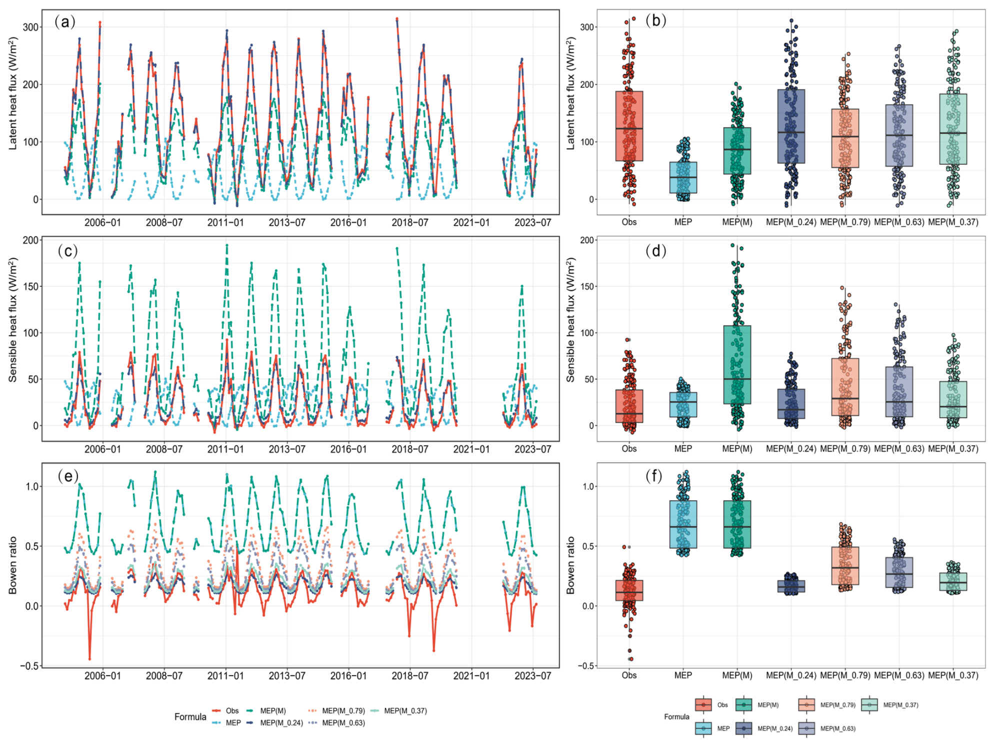

Figure 4. MEP model predicted latent heat flux (a), sensible heat flux (c), Bowen ratio (e) versus observations, and corresponding boxplots (b, d, f) of these variables at KEO site from June 17, 2004, to August 12, 2023. Note that the (a) and (c) only display results using MEP *(M_0.24)* among all four empirical Bowen ratio formulas for clearer comparison.

https://doi.org/10.5194/essd-2024-420
Preprint. Discussion started: 10 October 2024

For the variation pattern of the Bowen ratio, both the original MEP formula and the modified formulas exhibit consistent patterns with the observed values. The observed maximum Bowen ratio occurred in January 2005 (0.29), and the minimum in June 2005 (-0.4). However, the original MEP formula simulated a maximum of 1.01 and a minimum of 0.44, indicating a significant overestimation compared to the observed Bowen ratio. This discrepancy suggests that on the ocean surface, the available energy (R_n-G) is predominantly allocated to LE (Fig.S4). Among four empirical formulas, *M_0.24* simulated LE, H, and Bowen ratio values closest to the observed values. The median of the observed Bowen ratio was 0.11, while the original MEP Bowen ratio was 0.66. Among the four modified Bowen ratio formulas (*M_0.24*, *M_0.79*, *M_0.63*, *M_0.37*), their median Bowen ratios were 0.15, 0.32, 0.27, and 0.19 respectively, with *M_0.24* being the closest to the observed Bowen ratio.

Heat storage is crucial for the energy distribution process over the ocean surface. While the original MEP formulas have been effectively validated when applied to surfaces with shallow depths such as water and snow (Wang et al., 2014), they exhibit significant uncertainty when applied to the ocean surface. This discrepancy primarily arises from the fact that land is a non-transparent medium with relatively small heat storage values at monthly scales. Similarly, shallow water bodies also exhibit small heat storage values that can often be ignored. In the study by Wang et al. (2014), for example, two lakes with depths of 2m (Lake Tämnaren) and 4m (Lake Råksjö) still resulted in underestimated LE. However, for deeper lakes (generally > 3m depth), heat storage becomes significant and cannot be neglected (Zhao et al., 2016; Zhao & Gao, 2019). On deep ocean surfaces, with the most recent average depth estimate of 3,682 meters from NOAA satellite measurements, heat storage variations can influence depths up to 6,000 meters (Cheng et al., 2017). Therefore, the impact of heat storage is substantial and cannot be disregarded. In the original MEP theory, heat storage was not considered in the energy balance equation, where it was assumed that the net solar radiation (R_{ns}) is absorbed by the ocean and $R_{nL} = LE + H + Q$. Then, the heat storage was obtained as $G = R_{ns} + Q$. In this study, we compared the characteristics of MEP-derived G ($R_{ns} + Q$) with the observed G flux ($G = R_n - LE - H$ (Fig. S5). MEP-derived G shows a good correlation (R = 0.96) and consistent trends with the observed values (Fig. S5a & b), ranging from -4 to 81 W·m^{-2}. However, MEP-calculated Q (ranged from -210 to -65 W·m^{-2}) exhibits a negative correlation with the observed G (which ranged from -386 to 200 W·m^{-2}). Both MEP-derived G and Q fluxes are significantly underestimated. Therefore, the prediction errors in LE and H

https://doi.org/10.5194/essd-2024-420
Preprint. Discussion started: 10 October 2024

originates from the inability to accurately quantify heat storage. Hence, considering the influence of heat storage is crucial for accurately predicting LE and H over the ocean surface.

4.3 Evaluation of global radiation and heat storage flux

4.3.1 Evaluation of net radiation

After considering the effect of heat storage and the Bowen ratio, the improved MEP method demonstrated its high performance at the site scale. The results suggest that improved MEP method holds substantial promise for further application at a global scale. To facilitate this, we assessed the primary input variables of the improved MEP method (including R_n, G, and T_s) to identify datasets with the best accuracy.

Net radiation, as the primary variable in the energy balance equation, significantly influences the uncertainty of the MEP model (Huang et al., 2017). Selecting a reliable R_n product is essential for accurately estimating global latent and sensible heat fluxes. Previous studies have evaluated R_n at daily scales (Liang et al., 2022). In this study, we conducted a comprehensive evaluation of current mainstream monthly R_n products, including three remote sensing-based products (CERES, GEWEX-SRB, and JOFURO3) and two atmosphere reanalysis-based products (ERA5 and MERRA2). All products exhibited good consistency with buoy observations (Table 3 and Fig. S6), with R^2 values greater than 0.78. In terms of RMSE, the error rankings for all products were as: J-OFURO3 (10 W·m^{-2}) < ERA5 (39.03 W·m^{-2}) < CERES (40.67 W·m^{-2}) < GEWEX-SRB (41.83 W·m^{-2}) < MERRA2 (49.23 W·m^{-2}). It is evident that J-OFURO3 demonstrated the highest accuracy, as indicated by RMSE, NSE, and KGE statistics. This study is also consistent with previous assessments of global radiation (Liang et al., 2022), emphasizing J-OFURO3 as the least erroneous among all individual products and superior to existing alternatives including CERES4, ERA5, MERRA2, GEWEX-SRB, JRA55, OAFlux, and TropFlux.

Table 3. Evaluation of global monthly net radiation products against buoy observations

Products	R^2	ME (W·m^{-2})	MAE (W·m^{-2})	RMSE (W·m^{-2})	PBIAS (%)	NSE	KGE
J-OFURO3	**0.96**	**1.6**	**7.3**	**10.0**	**1.0**	**0.96**	**0.97**
ERA5	0.79	28.8	30.3	39.0	17.8	0.45	0.77
MERRA2	0.78	39.7	41.2	49.2	24.8	0.15	0.68
CERES	0.81	31.4	32.6	40.6	19.6	0.42	0.76
GEWEX-SRB	0.78	32.6	33.8	41.8	20.2	0.37	0.76

Note: The evaluation period for all datasets is 1988-2017, except for CERES, which spans from March 2000 to December 2017. The best-performed statistics are indicated in bold type.

https://doi.org/10.5194/essd-2024-420
Preprint. Discussion started: 10 October 2024

4.3.2 Evaluation of heat storage

The study underscores the importance of considering heat storage in simulating heat fluxes using the improved MEP model. For the first time, we assessed global heat storage using the J-OFURO3, ERA5, MERRA2, and ΔOHC datasets. In addition to assessing these individual datasets, we investigated the potential for enhancing accuracy through data fusion methods. We employed the BTCH and AA method to fuse heat storage data and compared the accuracy between individual datasets and fused datasets (Table 4). The results reveal that while using the AA method (e.g., AA4) to fuse yields smaller errors compared to ERA5, MERRA2, and ΔOHC, it still failed to achieve the accuracy of the J-OFURO3 product. Similarly, the BTCH method, despite fusing data from three or four sources, also does not match the accuracy of the J-OFURO3 method, as indicated by metrics of R^2, RMSE, and KGE. The heat storage derived from J-OFURO3 data shows high consistency with observations (R^2=0.95), as illustrated in Fig. 5 (spatial distribution of errors depicted in Fig.S7). Therefore, this study adopts the heat storage data derived from the J-OFURO3 dataset as the input for the MEP model.

To ensure consistency with radiation data source, the Sea surface temperature (SST) data from J-OFURO3 is utilized for T_s inputs, which is derived as the ensemble median from 12 global *SST* products (Tomita et al., 2019). Ultimately, the input variables including net radiation, heat storage, and sea surface temperature for driving MEP model are all determined from the J-OFURO3 dataset spanning from 1988 to 2017. Saturated specific humidity is computed as a function of *SST* and surface air pressure (from ERA5) using the Clausius-Clapeyron equation. The reliability of gridded data for the variables R_n, G, and T_s are simultaneously examined at an observational site (Fig.S8), where all three variables demonstrated high consistency with observed data from August 2004 to December 2017 (with $R^2 > 0.96$), effectively capturing the monthly dynamics of R_n, G, and T_s.

Table 4. Assessment of monthly heat storage between global remote sensing datasets and buoy observations

Products	R^2	ME ($W{\cdot}m^{-2}$)	MAE ($W{\cdot}m^{-2}$)	RMSE ($W{\cdot}m^{-2}$)	PBIAS (%)	NSE	KGE
J-OFURO3	**0.95**	**-3.5**	**15.3**	**19.7**	**-7.4**	**0.94**	**0.91**
ERA5	0.88	7.0	25.1	33.2	14.8	0.84	0.80
MERRA2	0.86	11.6	27.1	36.1	24.5	0.81	0.72
OHC	0.35	-48.2	64.4	86.9	-101.9	-0.11	-0.10

https://doi.org/10.5194/essd-2024-420
Preprint. Discussion started: 10 October 2024

BTCH3-1 (E M J)	0.89	7.1	22.8	30.5	15.1	0.86	0.81
BTCH3-2 (E M O)	0.88	4.6	24.0	31.4	9.9	0.85	0.86
BTCH4	0.91	5.9	19.7	26.2	12.5	0.90	0.86
AA2(EM)	0.87	9.3	25.4	34.1	19.7	0.83	0.76
AA3 (EMJ)	0.91	4.7	20.2	26.7	10.1	0.90	0.87
AA4 (E M J O)	0.91	11.5	21.4	28.6	24.4	0.88	0.74

Note: BTCH3-1 represents the fusion of three products (ERA5, MERRA2, and J-OFURO3) using the BTCH method; TCH3-2 represents the fusion of ERA5, MERRA2, and OHC; BTCH4 represents the fusion of ERA5, J-OFURO3, MERRA, and OHC. AA denotes the Simple Arithmetic Average (AA) method. The evaluation period spans from 1988 to 2017, and the best-performed statistics are indicated in bold type.

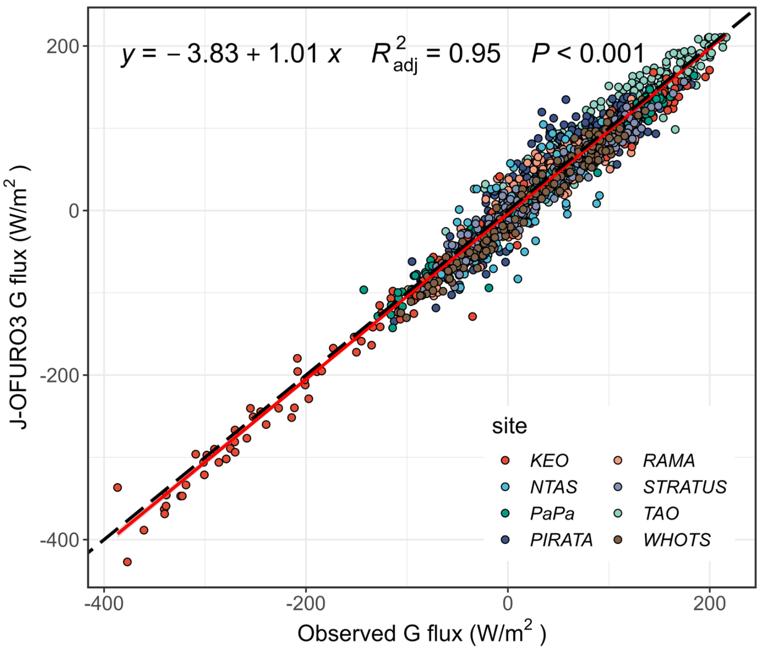

Figure 5. Assessment of heat storage (G) flux derived from remote sensed J-OFURO3 dataset against buoy observations. Distinct colors represent data from different buoy arrays.

4.4 Estimating long-term global ocean surface heat fluxes by improved MEP model

4.4.1 New estimate of global latent and sensible heat fluxes

After identifying the optimal driving dataset, this study employs the best-performed improved MEP method (i, e., *M_0.24*, hereinafter referred to as MEP for simplicity, while the original MEP formula is denoted as *MEP (ori)*) for global scale estimation, producing new estimations of latent and sensible heat fluxes for the period 1988-2017 (Table 5). The MEP model calculated the multi-year average *LE* as 92.87 W·m^{-2} and the

https://doi.org/10.5194/essd-2024-420
Preprint. Discussion started: 10 October 2024

sensible heat flux as 12.27 W·m^{-2} from 1988 to 2017. In comparison, LE ranges from 88.95 (OAFlux) to 100.54 W·m^{-2} (MERRA2), and *H* ranges from 10.17 (J-OFURO3) to 13.16 W·m^{-2} (MERRA2) for the other four products. The original MEP method yielded estimates of *LE* as 52.70 W·m^{-2} and *H* as 25.07 W·m^{-2}, significantly underestimating *LE* and overestimating *H* compared to estimates from other products. As previously demonstrated (Sections 4.1 & 4.2), the original MEP method overestimated *G* (42.20 W·m^{-2}) and exhibited notable deviations in the Bowen ratio. Therefore, the improved MEP method provides a more reasonable global estimation of LE and H.

Regarding the global spatial pattern (Fig.6), the MEP-derived latent heat shows higher values in low-latitude regions but notably decreases beyond 45° latitude. The highest LE values are observed in the southern Indian Ocean near Australia, the Pacific and Atlantic regions near South America, and the Indian Ocean near southern Africa. The peak values are observed within western boundary current systems (ranging from 200 to 260 W·m^{-2}), including the Gulf Stream in the North Atlantic and the Kuroshio in the western North Pacific. Impacted by the variations in oceanic currents near the equator, two general areas of higher *LE* have emerged (Yu et al., 2011), leading to notably low *LE* at the equator (88 W·m^{-2}), peaking at ~18°S at 132 W·m^{-2} (Fig. 6 & Fig.7). The MEP estimated *LE* exhibits a similar spatial pattern with other four products globally (Fig.6), particularly resembling OAFlux between 15°S and 15°N (Fig. 7). Overall, for the region between 30°S and 30°N, the ranking of LE values is as follows: OAFlux < MEP < J-OFURO3 < ERA5 < MERRA2, which is consistent with the magnitude of available energy. For sensible heat, MEP-derived H closely resembles that of ERA5 and MERRA2, with higher values predominantly occurred in two western boundary current systems, the South Indian Ocean near Australia area, and the Arctic Ocean. The improved MEP method mitigates the issue of overestimating *H* in mid-to-high latitudes compared to its original form (Fig.6l), resulting in more realistic spatial patterns. In high latitudes, J-OFURO3 exhibits higher H values than MEP and other comparable products in the Northern Hemisphere, with negative values observed between 45°S and 55°S. MEP generally estimates H within an intermediate range compared to other products, displaying a distribution that is more reasonable than that of J-OFURO3 product.

https://doi.org/10.5194/essd-2024-420
Preprint. Discussion started: 10 October 2024

Open Access Earth System Science Data Discussions

Table 5. Global area-averaged multi-annual mean estimates of latent heat flux

LE products	*LE* (W·m^{-2})	Evaporation (mm/yr)	*H* (W·m^{-2})	*G* (W·m^{-2})
MEP (0.24)	92.8	1195.5	12.2	19.7
ERA5	99.2	1277.8	12.0	34.2
MERRA2	100.5	1294.3	13.2	35.5
J-OFURO3	94.9	1222.2	10.1	19.7
OAflux	88.9	1145.1	10.4	/
MEP (ori)	52.7	678.5	25.1	42.2

Note: The period spans from 1988 to 2017. The MEP (0.24) denotes the improved MEP model, while MEP (ori) represents the original MEP model.

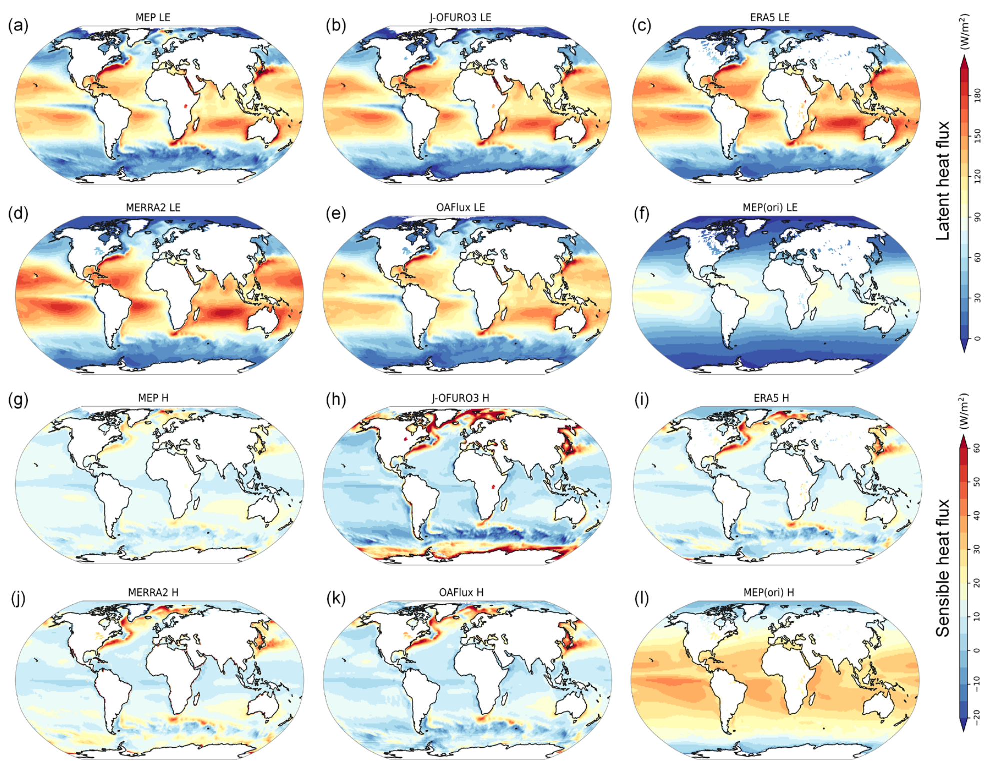

Figure 6. Global spatial maps of annual mean latent heat flux (*LE*) and sensible heat flux (*H*) during 1988-2017. Panels (a)-(f) depict latent heat flux derived from the improved MEP method, J-OFURO3, ERA5,

https://doi.org/10.5194/essd-2024-420
Preprint. Discussion started: 10 October 2024

Earth System Science Data
Open Access Discussions

MERRA2, OAFlux, and the original MEP method. Panels (g)-(l) show sensible heat flux from the same datasets.

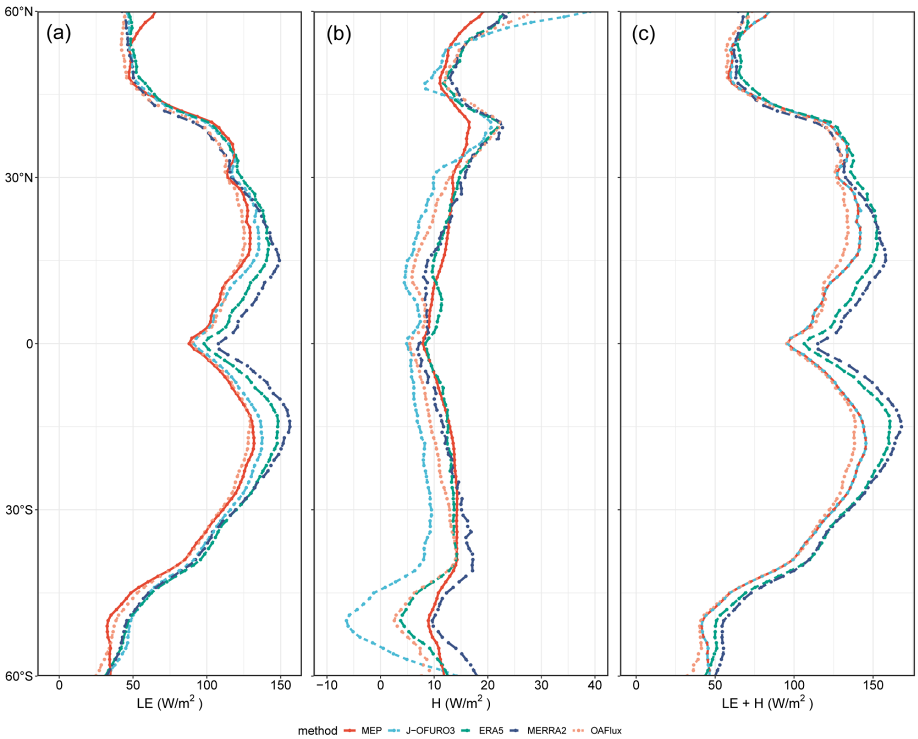

Figure 7. Meridional profiles of latent heat (left panel), sensible heat (middle panel) and their sum representing available energy (right panel) for the period 1988-2017.

4.4.2 Validation of global latent heat

To evaluate the disparity between MEP estimates of LE and those of other existing products, this study validated global-scale LE using 129 observational sites (as depicted in Fig.8 & Table 6). MEP-estimated LE showed strong consistency with buoy observations, achieving an R^2 of 0.79, a ME of 1.26 W·m^{-2}, and RMSE of 16 W·m^{-2}, all surpassing those of alternative products, underscoring its superior performance. Moreover, the MEP method exhibited superior performance with a higher NSE value of 0.77 and KGE of 0.89, demonstrating enhanced accuracy, reliability, and robustness. According to the RMSE evaluation criterion, the ranking of best-performed *LE* products is as: MEP, J-OFURO3, OAFlux, ERA5, MERRA2. In a recent comprehensive assessment of 15 global LE products (Tang et al., 2023), RMSE values ranged from 17.2 to

https://doi.org/10.5194/essd-2024-420
Preprint. Discussion started: 10 October 2024

45.3 W·m^{-2}, in which J-OFURO3 emerged as the best-performing product with the lowest RMSE of 17.2 W·m^{-2}, highest correlation coefficient (R) of 0.89, and ME of 6.5 W·m^{-2}. Studies have also shown minimal bias are given by J-OFURO3 on daily scale (Bentamy et al., 2017). This superior performance can be attributed to the use of continuously updated bulk algorithms (COARE 3.0 version) by J-OFURO3, the ongoing optimization of near-surface parameters (Tomita & Kubota, 2018), as well as the improved spatial resolution (0.25°). In this study, the improved MEP estimates of *LE* outperformed that of J-OFURO3, demonstrating higher accuracy and lower error (ME=1.26 W·m^{-2}), thereby establishing it as the most accurate global *LE* product currently available.

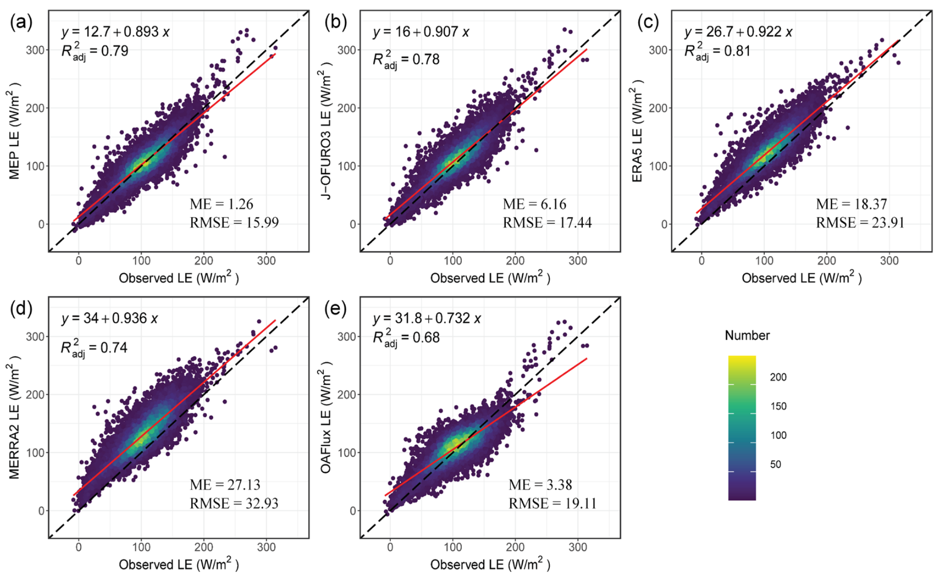

Figure 8. Scatter density plots of latent heat flux derived from distinct methods versus observations from 129 buoy stations during the period 1988-2017: (a) Improved MEP method, (b) J-OFURO3, (c) ERA5, (d) MERRA2, and (e) OAFlux. A total of 15444 records of latent heat observations are included.

Table 6. Evaluation of latent heat flux from different methods against buoy observations

Products	R^2	ME (W·m^{-2})	MAE (W·m^{-2})	RMSE (W·m^{-2})	PBIAS (%)	NSE	KGE
MEP	0.79	**1.3**	**12.2**	**15.9**	**1.2**	**0.77**	**0.89**
J-OFURO3	0.78	6.3	13.4	17.4	5.8	0.73	0.87
ERA5	**0.81**	18.4	19.9	23.9	17.3	0.48	0.80
MERRA2	0.74	27.1	28.1	32.9	25.5	0.02	0.70
OAFlux	0.68	3.4	14.9	19.1	3.2	0.67	0.79

Note: The evaluation period spans from 1988 to 2017, and the best-performed statistics are indicated in bold type.

https://doi.org/10.5194/essd-2024-420
Preprint. Discussion started: 10 October 2024

4.4.3 Comparisons of Bowen ratios

The improved MEP model achieves accurate LE estimates after refining the process of partitioning the surface energy budget, specifically through revisions to the Bowen ratio. The improved MEP method notably decreased the global-scale Bowen ratio, as illustrated in Fig. 9 and 10. Regarding latitude averages, the Bowen ratio of the original MEP formula ranged from 0.37 to 1.48 (with a median of 0.80), whereas the modified MEP Bowen ratio ranged from 0.09 to 0.35 (median of 0.18). Specifically, in the low-latitude region (10°S-10°N), the Bowen ratio of the modified MEP formula decreased from 0.37 to approximately 0.1, aligning closely with the Bowen ratios obtained from other reanalysis products (MERRA2, ERA5, OAFlux, and J-OFURO3). Globally, the median Bowen ratios of the products are as follows: MERRA2 (0.15), MEP (0.12), ERA5 (0.09), OAFlux (0.08), and J-OFURO3 (0.06). Spatially, the MEP Bowen ratio resembles ERA5 in mid to low latitudes but exhibits deviations from other products at high latitudes, where those products show fluctuating changes in the Bowen ratio (Fig.10). For instance, other products display abrupt transitions from negative to positive Bowen ratios in the Arctic and Antarctic regions, whereas MEP-derived values demonstrate greater stability in variations at higher latitudes. This discrepancy is likely due to the reanalysis products relying on the bulk method, which is sensitive to variations in wind speed and temperature gradients, leading to errors in simulating high wind speeds at the poles and causing fluctuations in latent and sensible heat. In contrast, the MEP model strictly adheres to energy conservation principles and operates independently of wind speed and temperature gradients, resulting in a more accurate estimate of the Bowen ratio. For example (Fig.S9), at the high-latitude PAPA buoy site (144.9°W, 50.1°N), the Bowen ratio estimated by MEP (median 0.24) closely matches the observed Bowen ratio (median 0.23). In contrast, all the other products underestimated the Bowen ratio, with J-OFURO3 (median -0.09) and OAFlux frequently exhibiting negative values. The Bowen ratio derived from MEP fits well with a Generalized Additive Model (GAM) (Fig.9). The implicit functional relationship between Bowen ratio and latitude is expressed as ($R^2 = 0.996$, $p < 0.001$): $B_{oa}\ (lat) = 0.207218 + f(lat) + \varepsilon$, where $f(lat)$ represents a smoothing function derived from a smooth curve, and ε denotes the error term. However, the specific functional form of $f(lat)$ cannot be explicitly determined. Therefore, a polynomial regression method is employed to explicitly fit B_{oa} and lat, resulting in ($R^2 = 0.91$, $p < 0.001$): $B_{oa} = 9.97 \times 10^{-2} - 3.45 \times 10^{-4} \times lat + 4.71 \times 10^{-5} \times lat^2 + \varepsilon$ (as in Fig.S10). This equation serves as a reference for partitioning surface energy over data-sparse oceanic regions.

https://doi.org/10.5194/essd-2024-420
Preprint. Discussion started: 10 October 2024

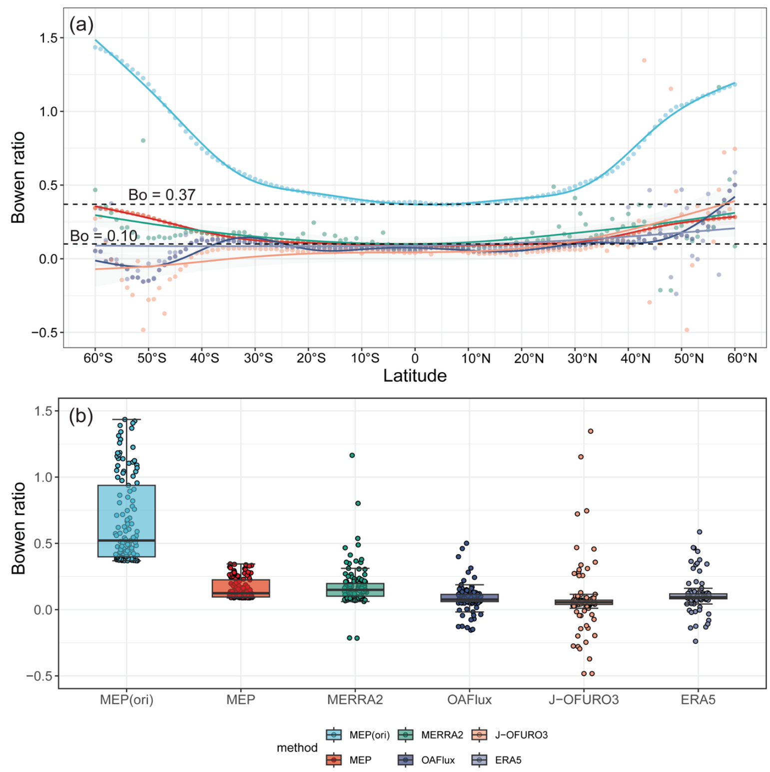

Figure 9. Global ocean latitudinal averaged Bowen ratio derived by the MEP method and four other products from 1988 to 2017. (a) Latitudinal averaged Bowen ratio derived from the MEP model using original and modified Bowen ratio formulas, with points fitted by a generalized additive model (GAM). (b) Statistical distribution of the latitudinal annual mean Bowen ratio.

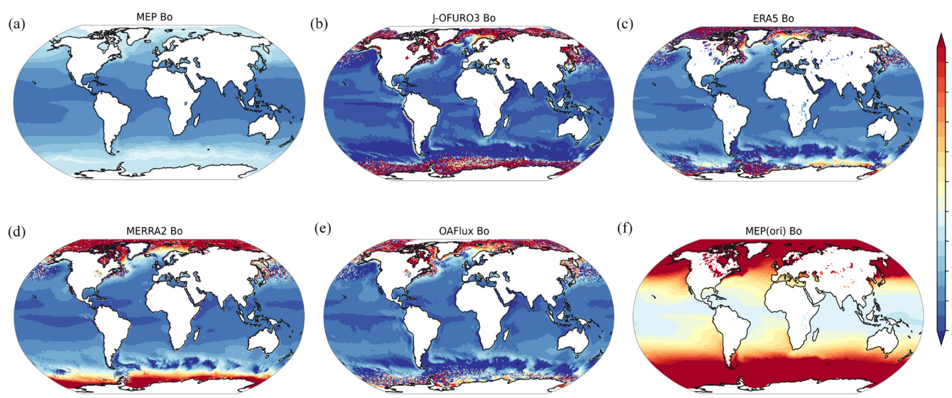

Figure 10. Global distribution of ocean annual mean Bowen ratio during 1988-2017: (a) Improved MEP method, (b) J-OFURO3, (c) ERA5, (d) MERRA2, (e) OAFlux, and (f) MEP original method.

https://doi.org/10.5194/essd-2024-420
Preprint. Discussion started: 10 October 2024

4.5 Spatial-temporal variability of ocean evaporation

Heat flux reflects the energy exchange between the ocean and the atmosphere, while evaporation (*ET*) reflects moisture exchange within the water cycle. The spatiotemporal patterns of evaporation were analyzed using Sen's slope and the Mann-Kendall test methods (Fig.11). Globally, approximately 74% (with 27% statistically significant) showed an increasing trend, while 26% (with 21% statistically significant) exhibited a decreasing trend. The regions with the highest increasing trends were predominantly observed near western boundary current systems, the convergence zones of the East Australian Current and the South Equatorial Current, and the convergence zones of the Eastern South Equatorial Current and the Brazil Current along South America. Decreasing trends were primarily observed in equatorial regions of the Pacific and Atlantic Oceans, as well as near the Labrador and Kuroshio currents and north of the Antarctic Circle. It is indicated that regions with significant increases (decreases) in evaporation generally correspond closely to the distribution of major warm currents (cold currents) spatially.

Over the multi-year changes from 1988 and 2017, MEP, J-OFURO3, ERA5, and MERRA2 all exhibited significant increasing trends in *ET*. MEP estimated an evaporation increased rate of 2.31 mm/year, whereas OAFlux showed a non-significant trend (Fig.12). This upward trend in ET can largely be attributed to changes in available energy, which increased at a rate of 0.274 W/(m^2·year). For instance, during peak *ET* years such as 1989, 1992, 2003, and 2008, R_n was also at its highest; conversely, during years of minimum *ET* like 1991 and 1997, R_n was minimal. This consistency is in line with previous findings (Huang et al., 2017), where more than 50% of the uncertainty in MEP-modeled fluxes was attributed to the radiation term. While different methods yield varying magnitudes of *ET* changes, they generally exhibit a transition around 2010: an increasing trend from 1988 to around 2010 followed by a decreasing trend thereafter (Fig. 12a). For instance, MEP indicated an ET increase of 3.58 mm/year from 1988 to 2010, followed by a decrease at a rate of 2.18 mm/year after 2010. This shift primarily results from a decline in both available energy and surface temperature starting around 2010. Although T_s increased after 2012, the significant decrease in available energy was the main driver behind the decline in *ET*.

https://doi.org/10.5194/essd-2024-420
Preprint. Discussion started: 10 October 2024

Earth System Science Data
Open Access
Discussions

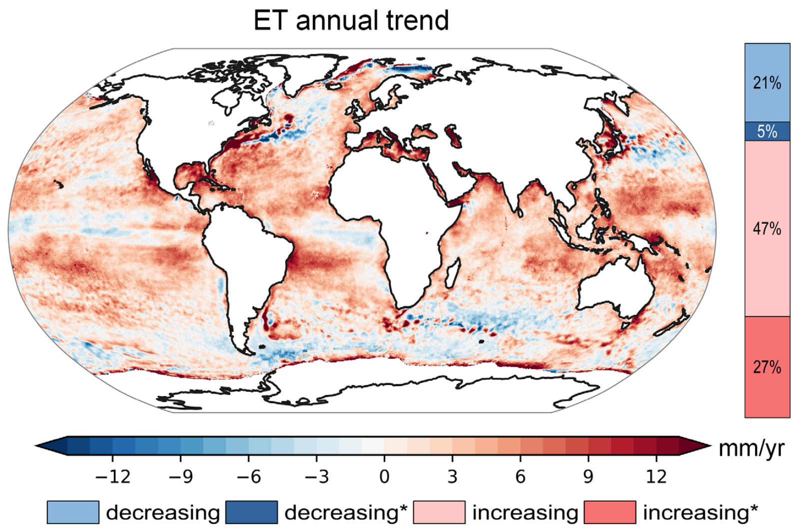

Figure 11. Spatial distribution of the long-term trend in the annual mean ocean evaporation derived from the improved MEP method during 1988-2017.

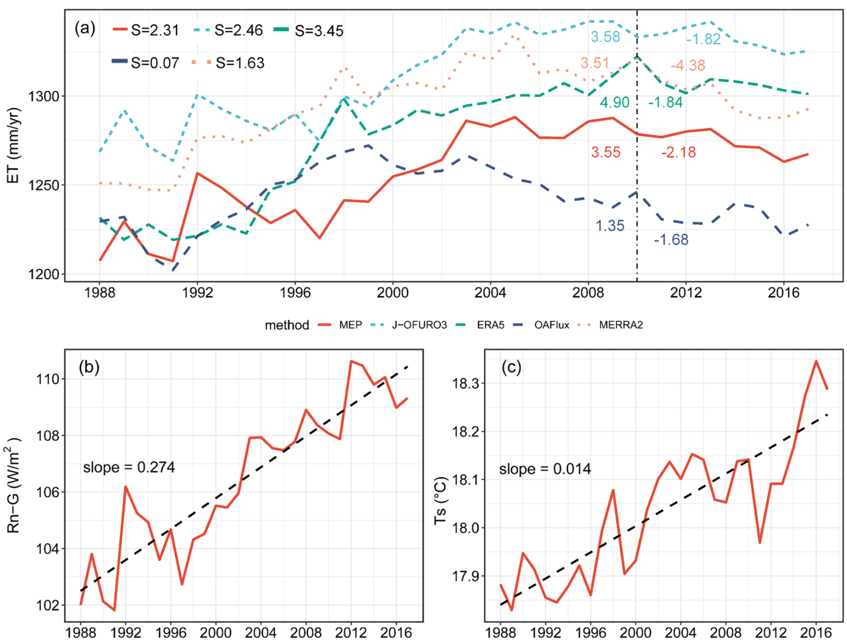

Figure 12. Time series of area-averaged multi-annual mean evaporation from the improved MEP method (a), available energy (b), and sea surface temperature (c) over the global oceans during 1988-2017. The black dotted line in panel (a) represents year 2010, and the black dashed lines in panels (b) and (c) represent the linear regression lines.

https://doi.org/10.5194/essd-2024-420
Preprint. Discussion started: 10 October 2024

5. Discussion

5.1 Quantifying impact of heat storage and radiation with sensitivity analysis

The sensitivity analysis reveals the significant influence of input variables on latent heat flux derived from the MEP model. Notably, the heat storage (G) exhibits seasonal variations with both positive and negative values (Fig. 13). Positive G values coincide predominantly with summer in the Northern Hemisphere (winter in the Southern Hemisphere), specifically from June to August (Fig. 4 and Fig. S5). During this season, intensified solar radiation enhances the net energy input (R_n) at the ocean surface, leading to heat absorption and retention. Consequently, the energy available (R_n - G) for evaporation diminishes. The analysis indicates that R_n significantly influences the energy-driven evaporation process, with a sensitivity coefficient exceeding 1 (median 1.74), highlighting its pivotal role. In contrast, G negatively impacts evaporation, as indicated by a sensitivity coefficient of -0.74. Specific humidity (median 0.08) and sea surface temperature have relatively minor effects, consistent with previous MEP model findings focused on terrestrial surfaces (Isabelle et al., 2021).

Conversely, negative values of heat storage predominate during winter, particularly from December to February in the Northern Hemisphere (June to August in the Southern Hemisphere). Despite reduced solar radiation during this period, residual heat stored from summer gradually releases into the atmosphere, resulting in greater energy output than input. This surplus energy augments the available energy for evaporation, leading to a positive sensitivity coefficient for G (median 0.29), second only to R_n (median 0.71). Consequently, this process generally reduces sea surface temperature, resulting in a negative sensitivity coefficient for surface temperature. Overall, these findings underscore the significant influence of R_n on latent heat flux, with G ranking as the second most influential variable in MEP estimates over ocean surfaces. For instance, a 10% decrease in positive G yields a 7.4% increase in evaporation, while a 10% increase in negative G results in a 2.9% increase in evaporation, assuming other variables remain constant. Thus, R_n and G emerge as primary drivers of oceanic evaporation, with humidity and temperature exerting minimal influence.

Furthermore, the pivotal role of available energy in determining LE is underscored by its direct relationship with energy allocation. Thus, the accuracy of available energy estimates directly influences LE simulations. Despite using bulk methods (COARE 3.0 algorithms) independent of radiation partitioning,

https://doi.org/10.5194/essd-2024-420
Preprint. Discussion started: 10 October 2024

discrepancies in *LE* simulations correlate with errors in available energy estimates (Tables 3 and 4). Notably, the MERRA2 product exhibited higher errors in simulating R_n and G compared to observations, leading to significant biases in *LE* estimation. In contrast, ERA5 product demonstrated superior performance in simulating R_n and G, thereby achieving higher accuracy in *LE* estimation. Consequently, the energy-balance-based MEP model excels in accurately computing surface heat fluxes by directly reflecting energy allocation. Unlike bulk methods, the MEP approach reduces sensitivity to temperature and humidity gradients, thereby minimizing uncertainties in *LE* simulations (Pelletier et al., 2018). This advancement enhances the MEP model's utility in global energy and water cycle research, particularly pertinent for future climate change studies.

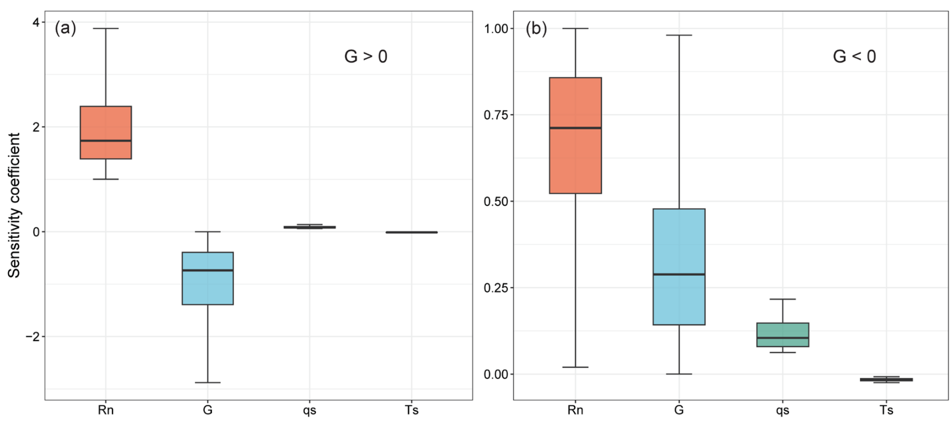

Figure 13. Sensitivity coefficient associated with inputs variables for the improved MEP method at all 129 buoy stations: (a) for positive *G* values, and (b) for negative *G* values.

5.2 Discrepancy of empirical Bowen ratio formulas

Bowen ratio plays a crucial role in understanding the surface energy partitioning process. In this study, four empirical formulas were utilized to modify the MEP model and were evaluated against observations of latent heat flux, each with distinct conditions of applicability and suitability for integration with the MEP model: (1) B_{oa}=0.63B_o^*-0.15 is derived from direct observational data fitting (Hicks and Hess, 1977). This formula is applicable for surface temperatures above 16°C, particularly within latitudes between 40°N and 40°S, making it more suitable for lower latitude regions. Therefore, it is more suitable for lower latitude regions; (2) B_{oa}=0.79B_o^*-0.21 is derived using the Priestley–Taylor model under advection-free conditions (Priestley and Taylor, 1972). The coefficients are based on a mean α value of 1.26 (although this varies in practice). However, recent studies have shown significant discrepancies due to the neglect of the interaction between R_n and T_s variations (Yang & Roderick, 2019); (3) B_{oa}=0.24B_o^* was developed to address this limitation based on a maximum evaporation theory by considering the feedback mechanism between R_n and T_s (under the circumstances of G to be small to negligible). The empirical coefficient (0.24) was determined by fitting Bowen ratio and surface temperature data across the global ocean surface (Yang & Roderick, 2019); and (4) B_{oa}=0.37B_o^*-0.05 was subsequently formulated based on principles derived from atmospheric boundary layer (ABL) theory (Liu & Yang, 2021), with coefficients also fitted from relationships between B_{oa} and T_s. It should be noted that the derivations of B_{oa}=0.24B_o^* and B_{oa}=0.37B_o^*-0.05 were based on fitting using latent heat data from the OAFlux dataset rather than direct buoy observations. Building upon the four empirical relationships between B_{oa} and B_o^* from previous studies, this study assessed the applicability of these four empirical Bowen ratio formulas in estimating latent heat flux. The findings indicate that the MEP model refined with B_{oa}=0.24B_o^*, exhibits superior accuracy at both localized and global scales, effectively mitigating the underestimation of LE in its original formulation. Moreover, the results show that the improved MEP model closely aligns with buoy observations and achieves higher accuracy globally compared to OAFlux products (as depicted in Fig. 8), surpassing other bulk method-based products as well.

5.3 Contributions and implications of this study

The main contributions of this study include: (1) The MEP model's energy balance equation over water surfaces was revised to explicitly consider heat storage effect. This correction highlights the importance of heat storage in estimating latent heat flux. (2) The energy partitioning of the MEP model was revised to incorporate empirical Bowen ratio formulas, significantly improving the heat flux estimations. (3) This study conducted the first thorough global assessment of heat storage using extensive buoy observations and remote sensed data, enabling the MEP model to produce the most accurate global latent heat flux estimates. This study addresses the issue of underestimating latent heat flux by the MEP model, increasing the global average LE from 53 W·m^{-2} to 93 W·m^{-2}, while reducing sensible heat flux from 25 W·m^{-2} to 12 W·m^{-2}, improving the partitioning of energy budget. The improved MEP model provides precise LE estimates compared to existing datasets like J-OFURO3, ERA5, MERRA2, and OAFlux, enabling it to become a valuable benchmark dataset for global evaporation studies.

https://doi.org/10.5194/essd-2024-420
Preprint. Discussion started: 10 October 2024

From a methodological perspective, the improved MEP method presents a new approach for estimating heat flux that diverges from existing bulk methods. The bulk method traditionally requires input parameters including air temperature, specific humidity, wind speed, sea surface temperature, and atmospheric pressure, as well as the observational height of all parameters (Fairal et al., 2003; Tomita et al., 2021). In contrast to the bulk method, which requires a high demand for driving variables and shows lower sensitivity to temperature variations. It requires only net radiation, heat storage, and surface temperature to simultaneously estimate latent heat and sensible heat fluxes. Furthermore, the improved MEP model is not constrained by the magnitude of heat storage and theoretically can be applied across various temporal scales (including sub-daily and daily), beyond the monthly scale used in this study. This underscores the applicability of the MEP method in addressing the constraints of traditional bulk methods, providing another independent approach to estimating heat fluxes across diverse environmental conditions.

This study applies the improved MEP model to ocean surface, with potential for future extension to lake and reservoir surfaces. Compared to the Penman model for water body evaporation (Tian et al., 2022; Zhao et al., 2022; Bai et al., 2023), major advantage of MEP method lies in its independence from wind speed, as long as the heat storage can be determined using an equilibrium temperature-based approach (McMahon et al., 2013; Zhao & Gao, 2019). The global LE dataset generated in this study, given MEP's insensitivity to variations in air temperature and humidity, can be applied in studies related to ocean salinity (Liu et al., 2019), ocean warming (Cheng et al., 2022), global climate change and water cycle research (Konapala et al., 2020).

6. Data availability

The dataset produced using the MEP method, which includes global latent heat flux and sensible heat flux at a monthly scale from 1988 to 2017, can be freely downloaded from the Figshare platform (https://doi.org/10.6084/m9.figshare.26861767.v2, Yang et al., 2024). All the datasets used in this study are publicly available online and are described in the Data Materials section.

7. Conclusions

In this study, we developed a global monthly latent heat flux product for the ocean covering the period from 1988 to 2017. This product is based on a maximum entropy production theory framework, incorporating heat storage and Bowen ratio optimizations. It represents the first energy-balance-based dataset that differs from existing global ocean heat flux datasets derived from bulk methods. To assess the accuracy of the input variables for the maximum entropy production framework, we utilized five global datasets, including two remote sensing-based and three from reanalysis-based, alongside four global datasets of heat storage derived from the energy balance equation and ocean heat content changes. We employed data fusion methods, including arithmetic averaging and the Bayesian three-cornered hat method, to identify optimal input datasets through validation against observations. The performance of the newly produced dataset was evaluated against extensive observations from 129 globally distributed buoy stations using multiple statistical metrics, and it was also compared with four auxiliary products: J-OFURO3, ERA5, MERRA2, and OAFlux. Additionally, we analyzed the long-term spatial-temporal variability of ocean latent heat flux. Ultimately, we investigated the impacts of ocean heat storage, net radiation, and Bowen ratio changes on heat flux estimations and surface energy partitioning.

The MEP framework provides new estimates of global heat fluxes. The MEP-estimated long-term annual mean latent heat flux is 93 $W\cdot m^{-2}$ (equivalent to 1196 mm/year of evaporation) during the period from 1988 to 2017. This estimate is at an intermediate level compared to other global flux products, which range from 90 $W\cdot m^{-2}$ (OAFlux) to 101 $W\cdot m^{-2}$ (MERRA2). The MEP-estimated sensible heat flux is 12 $W\cdot m^{-2}$, falling within the range of 10.17 $W\cdot m^{2}$ (J-OFURO3) to 13 $W\cdot m^{2}$ (MERRA2) reported by other current products. Compared with previous heat flux products, the MEP-estimated latent heat demonstrated higher accuracy when validated against observations, with a ME of 1.26 $W\cdot m^{-2}$, a RMSE of 16 $W\cdot m^{-2}$, and a KGE value of 0.89, outperforming all other contemporary global products. Approximately 74% of oceanic regions experienced an increasing trend in evaporation from 1988 to 2017. Regarding long-term temporal variability, the global annual mean evaporation exhibited an increase rate of 3.58 mm/yr from 1988 to 2010 but subsequently decreased at a rate of 2.18 mm/yr from 2010 to 2017, which was consistent with changes in surface available energy.

This study demonstrates that the improved MEP framework has significantly improved the accuracy of the original MEP theory, addressing both the underestimation of latent heat and the overestimation of sensible heat flux. This improvement was achieved by incorporating the impact of heat storage and modifying the Bowen ratio formula within the MEP theory. The consideration of heat storage resolved the issue of seasonal

https://doi.org/10.5194/essd-2024-420
Preprint. Discussion started: 10 October 2024

phase mismatches (approximately 6-month lags) between MEP estimates and buoy observations. Building upon this improvement, this study further optimized the energy partitioning process by correcting the Bowen ratio, linearly adjusting the equilibrium Bowen ratio to align with actual conditions. Four empirical Bowen ratio formulas for modifying the MEP method were assessed globally, identifying B_{oa}=0.24B_o^* as the most accurate formula for estimating latent heat flux within MEP method. The impact of heat storage on estimating heat fluxes was quantified through the sensitivity analysis. Net radiation and heat storage were identified as the primary drivers of evaporation estimates. A 10% decrease in positive heat storage led to a 7.4% increase in evaporation, whereas a 10% increase in negative heat storage resulted in a 2.9% increase.

Compared to existing bulk methods, the MEP model offers several advantages including the need for fewer input variables, independence from wind speed, and insensitivity to variations in temperature and humidity. The MEP derived ocean heat flux dataset has been validated and provides accurate estimates of latent heat flux. Additionally, this MEP method can be applied to estimate evaporation from other deep-water surfaces, such as lakes and reservoirs where heat storage is significant. Overall, the MEP-derived ocean heat flux dataset provides high global accuracy, fine spatial resolution (0.25°), and extensive long-term temporal records. This dataset is expected to be valuable for applications related to global ocean warming, hydrological cycles, and their interactions with other Earth system components in the context of climate change.

https://doi.org/10.5194/essd-2024-420
Preprint. Discussion started: 10 October 2024

Supplement. The Supplementary material related to this article is submitted during submission.

Author contributions. YY and HS developed the methodology and designed the experiments, WZ contributed the conceptual design, YY and WZ collected and processed the data, YY wrote the first draft of the paper under the supervision of other authors. All authors participated in the revies and editing of the paper.

Competing interests. The contact author has declared that none of the authors has any competing interests.

Acknowledgments. We acknowledge the GTMBA Project Office of NOAA/PMEL for providing the Global Tropical Moored Buoy Array observations. This study was primarily funded by the Third Xinjiang Scientific Expedition Program (Grant No.2022xjkk0105) (H.S.). The authors acknowledge funding from the NSFC project (52079055, 52011530128). H.S. and W.Z. acknowledges funding from the NSFC-STINT projects (No. 202100-3211 and CH2019-8281). W. Z. was supported by the grants from Swedish Research Council VR (2020-05338), and Swedish National space Agency (209/19).

https://doi.org/10.5194/essd-2024-420
Preprint. Discussion started: 10 October 2024

References

Andreas, E. L., & Cash, B. A.: A new formulation for the Bowen ratio over saturated surfaces. Journal of Applied Meteorology and Climatology, 35(8), 1279-1289, 1996.

Andreas, E. L., Jordan, R. E., Mahrt, L., & Vickers, D.: Estimating the Bowen ratio over the open and ice-covered ocean. Journal of Geophysical Research: Oceans, 118(9), 4334-4345, 2013.

Andreas, E. L., Persson, P. O. G., & Hare, J. E.: A bulk turbulent air–sea flux algorithm for high-wind, spray conditions. Journal of Physical Oceanography, 38(7), 1581-1596, 2008.

Bai, P., & Guo, X.: Development of a 60-year high-resolution water body evaporation dataset in China. Agricultural and Forest Meteorology, 334, 109428, 2023.

Bentamy, A., Piolle, J. F., Grouazel, A., Danielson, R., Gulev, S., Paul, F., ... & Josey, S. A.: Review and assessment of latent and sensible heat flux accuracy over the global oceans. Remote Sensing of Environment, 201, 196-218, 2017.

Beven, K.: A sensitivity analysis of the Penman-Monteith actual evapotranspiration estimates. Journal of Hydrology, 44(3–4), 169-190, 1979.

Bosilovich, M. G., Robertson, F. R., & Chen, J.: Global energy and water budgets in merra. Journal of Climate, 24(22), 5721-5739, 2011.

Bourras, D.: Comparison of five satellite-derived latent heat flux products to moored buoy data. Journal of Climate, 19(24), 6291-6313, 2006.

Chen, X., Yao, Y., Li, Y., Zhang, Y., Jia, K., Zhang, X., ... & Guo, X.: ANN-based estimation of low-latitude monthly ocean latent heat flux by ensemble satellite and reanalysis products. Sensors, 20(17), 4773, 2020.

Cheng, L., Pan, Y., Tan, Z., Zheng, H., Zhu, Y., Wei, W., ... & Zhu, J.: IAPv4 ocean temperature and ocean heat content gridded dataset. Earth System Science Data Discussions, 2024, 1-56, 2024.

Cheng, L., Trenberth, K. E., Fasullo, J., Boyer, T., Abraham, J., & Zhu, J.: Improved estimates of ocean heat content from 1960 to 2015. Science Advances, 3(3), e1601545, 2017.

Cheng, L., von Schuckmann, K., Abraham, J. P., Trenberth, K. E., Mann, M. E., Zanna, L., ... & Lin, X.: Past and future ocean warming. Nature Reviews Earth & Environment, 3(11), 776-794, 2022.

Duan, S. B., Zhou, S., Li, Z. L., Liu, X., Chang, S., Liu, M., ... & Shang, G.: Improving monthly mean land surface temperature estimation by merging four products using the generalized three-cornered hat method and maximum likelihood estimation. Remote Sensing of Environment, 302, 113989, 2024.

Fairall, C. W., Bradley, E. F., Hare, J. E., Grachev, A. A., & Edson, J. B.: Bulk parameterization of air–sea fluxes: Updates and verification for the COARE algorithm. Journal of climate, 16(4), 571-591, 2003.

Fairall, C. W., Bradley, E. F., Rogers, D. P., Edson, J. B., & Young, G. S.: Bulk parameterization of air-sea fluxes for tropical ocean-global atmosphere coupled-ocean atmosphere response experiment. Journal of Geophysical Research: Oceans, 101(C2), 3747-3764, 1996.

https://doi.org/10.5194/essd-2024-420
Preprint. Discussion started: 10 October 2024

Gelaro, R., McCarty, W., Suárez, M. J., Todling, R., Molod, A., Takacs, L., ... & Zhao, B.: The modern-era retrospective analysis for research and applications, version 2 (MERRA-2). Journal of climate, 30(14), 5419-5454, 2017.

Guo, J., Li, W., Chang, X., Zhu, G., Liu, X., & Guo, B.: Terrestrial water storage changes over Xinjiang extracted by combining Gaussian filter and multichannel singular spectrum analysis from GRACE. Geophysical Journal International, 213(1), 397-407, 2018.

He, X., Xu, T., Xia, Y., Bateni, S. M., Guo, Z., Liu, S., ... & Zhao, J.: A Bayesian three-cornered hat (BTCH) method: improving the terrestrial evapotranspiration estimation. Remote Sensing, 12(5), 878, 2020.

Hersbach, H., Bell, B., Berrisford, P., Hirahara, S., Horányi, A., Muñoz-Sabater, J., ... & Thépaut, J. N.: The ERA5 global reanalysis. Quarterly Journal of the Royal Meteorological Society, 146(730), 1999-2049, 2020.

Hicks, B. B., & Hess, G. D.: On the Bowen ratio and surface temperature at sea. Journal of physical oceanography, 7(1), 141-145, 1977.

Huang, S. Y., Deng, Y., & Wang, J.: Revisiting the global surface energy budgets with maximum-entropy-production model of surface heat fluxes. Climate Dynamics, 49, 1531-1545, 2017.

Isabelle, P. E., Viens, L., Nadeau, D. F., Anctil, F., Wang, J., & Maheu, A.: Sensitivity analysis of the maximum entropy production method to model evaporation in boreal and temperate forests. Geophysical Research Letters, 48(13), e2020GL091919, 2021.

Iwasaki, S., Kubota, M., & Watabe, T.: Assessment of various global freshwater flux products for the global ice-free oceans. Remote sensing of environment, 140, 549-561, 2014.

Jo, Y. H., Yan, X. H., Pan, J., He, M. X., & Liu, W. T.: Calculation of the Bowen ratio in the tropical Pacific using sea surface temperature data. Journal of Geophysical Research: Oceans, 107(C9), 17-1, 2002.

Johnson, G. C., & Lyman, J. M.: Warming trends increasingly dominate global ocean. Nature Climate Change, 10(8), 757-761, 2020.

Konapala, G., Mishra, A. K., Wada, Y., & Mann, M. E.: Climate change will affect global water availability through compounding changes in seasonal precipitation and evaporation. Nature communications, 11(1), 3044, 2020.

Lenhart, T., Eckhardt, K., Fohrer, N., & Frede, H. G.: Comparison of two different approaches of sensitivity analysis. Physics and Chemistry of the Earth, Parts A/B/C, 27(9-10), 645-654, 2002.

Li, Z., England, M. H., & Groeskamp, S.: Recent acceleration in global ocean heat accumulation by mode and intermediate waters. Nature Communications, 14(1), 6888, 2023.

Liang, H., Jiang, B., Liang, S., Peng, J., Li, S., Han, J., ... & Zhang, X.: a global long-term ocean surface daily/0.05 net radiation product from 1983–2020. Scientific Data, 9(1), 337, 2022.

Liu, C., Liang, X., Ponte, R. M., Vinogradova, N., & Wang, O.: Vertical redistribution of salt and layered changes in global ocean salinity. Nature communications, 10(1), 3445, 2019.

https://doi.org/10.5194/essd-2024-420
Preprint. Discussion started: 10 October 2024

Liu, J., Chai, L., Dong, J., Zheng, D., Wigneron, J. P., Liu, S., ... & Lu, Z.: Uncertainty analysis of eleven multisource soil moisture products in the third pole environment based on the three-corned hat method. Remote sensing of environment, 255, 112225, 2021.

Liu, Z., & Yang, H.: Estimation of water surface energy partitioning with a conceptual atmospheric boundary layer model. Geophysical Research Letters, 48(9), e2021GL092643, 2021.

Long, D., Pan, Y., Zhou, J., Chen, Y., Hou, X., Hong, Y., ... & Longuevergne, L.: Global analysis of spatiotemporal variability in merged total water storage changes using multiple GRACE products and global hydrological models. Remote sensing of environment, 192, 198-216, 2017.

Marti, F., Blazquez, A., Meyssignac, B., Ablain, M., Barnoud, A., Fraudeau, R., ... & Benveniste, J.: Monitoring the ocean heat content change and the Earth energy imbalance from space altimetry and space gravimetry. Earth System Science Data, 14(1), 229-249, 2022.

Masson-Delmotte V, Zhai P, Pirani S, Connors C, Péan S, Berger N, et al.: IPCC, 2021: Summary for policymakers. in: Climate change 2021: The physical science basis. contribution of working group I to the sixth assessment report of the intergovernmental panel on climate change, 2021.

McMahon, T. A., Peel, M. C., Lowe, L., Srikanthan, R., & McVicar, T. R.: Estimating actual, potential, reference crop and pan evaporation using standard meteorological data: a pragmatic synthesis. Hydrology and Earth System Sciences, 17(4), 1331-1363, 2013.

Meehl, G. A.: A calculation of ocean heat storage and effective ocean surface layer depths for the Northern Hemisphere. Journal of physical oceanography, 14(11), 1747-1761, 1984.

Pelletier, C., Lemarié, F., & Blayo, E.: Sensitivity analysis and metamodels for the bulk parametrization of turbulent air–sea fluxes. Quarterly Journal of the Royal Meteorological Society, 144(712), 658-669, 2018.

Philip, J.R.: A physical bound on the Bowen ratio. Journal of Climate and Applied Meteorology, 26, 1043–1045, 1987.

Pinker, R. T., & Laszlo, I.: Modeling surface solar irradiance for satellite applications on a global scale. Journal of Applied Meteorology and Climatology, 31(2), 194-211, 1992.

Pokhrel, S., Dutta, U., Rahaman, H., Chaudhari, H., Hazra, A., Saha, S. K., & Veeranjaneyulu, C.: Evaluation of different heat flux products over the tropical Indian Ocean. Earth and Space Science, 7(6), e2019EA000988, 2020.

Priestley, C. H. B., & Taylor, R. J.: On the assessment of surface heat flux and evaporation using large-scale parameters. Monthly weather review, 100(2), 81-92, 1972.

Robertson, F. R., Roberts, J. B., Bosilovich, M. G., Bentamy, A., Clayson, C. A., Fennig, K., ... & Slivinski, L. C.: Uncertainties in ocean latent heat flux variations over recent decades in satellite-based estimates and reduced observation reanalyses. Journal of Climate, 33(19), 8415-8437, 2020.

Roderick, M. L., Sun, F., Lim, W. H., & Farquhar, G. D.: A general framework for understanding the response of the water cycle to global warming over land and ocean. Hydrology and Earth System Sciences, 18(5), 1575-1589, 2014.

https://doi.org/10.5194/essd-2024-420
Preprint. Discussion started: 10 October 2024

Rutan, D. A., Kato, S., Doelling, D. R., Rose, F. G., Nguyen, L. T., Caldwell, T. E., & Loeb, N. G.: CERES synoptic product: Methodology and validation of surface radiant flux. Journal of Atmospheric and Oceanic Technology, 32(6), 1121-1143, 2015.

Shaman, J., & Kohn, M.: Absolute humidity modulates influenza survival, transmission, and seasonality. Proceedings of the National Academy of Sciences, 106(9), 3243-3248, 2009.

Shao, X., Zhang, Y., Liu, C., Chiew, F. H., Tian, J., Ma, N., & Zhang, X.: Can indirect evaluation methods and their fusion products reduce uncertainty in actual evapotranspiration estimates?. Water Resources Research, 58(6), e2021WR031069, 2022.

Smith, S. R., Hughes, P. J., & Bourassa, M. A.: A comparison of nine monthly air–sea flux products. International Journal of Climatology, 31(7), 1002-1027, 2011.

Sun, H., Chen, J., Yang, Y., Yan, D., Xue, J., Wang, J., & Zhang, W.: Assessment of long-term water stress for ecosystems across China using the maximum entropy production theory-based evapotranspiration product. Journal of Cleaner Production, 349, 131414, 2022.

Sun, H., Sun, X., Chen, J., Deng, X., Yang, Y., Qin, H., ... & Zhang, W.: Different types of meteorological drought and their impact on agriculture in Central China. Journal of Hydrology, 627, 130423, 2023.

Tang, R., Wang, Y., Jiang, Y., Liu, M., Peng, Z., Hu, Y., ... & Li, Z. L.: A review of global products of air-sea turbulent heat flux: accuracy, mean, variability, and trend. Earth-Science Reviews, 104662, 2023.

Tian, W., Liu, X., Wang, K., Bai, P., Liu, C., & Liang, X.: Estimation of global reservoir evaporation losses. Journal of Hydrology, 607, 127524, 2022.

Tomita, H., Hihara, T., & Kubota, M.: Improved satellite estimation of near-surface humidity using vertical water vapor profile information. Geophysical Research Letters, 45(2), 899-906, 2018.

Tomita, H., Hihara, T., Kako, S. I., Kubota, M., & Kutsuwada, K.: An introduction to J-OFURO3, a third-generation Japanese ocean flux data set using remote-sensing observations. Journal of Oceanography, 75(2), 171-194, 2019.

Tomita, H., Kutsuwada, K., Kubota, M., & Hihara, T.: Advances in the estimation of global surface net heat flux based on satellite observation: J-OFURO3 V1. 1. Frontiers in Marine Science, 8, 612361, 2021.

Von Schuckmann, K., Minière, A., Gues, F., Cuesta-Valero, F. J., Kirchengast, G., Adusumilli, S., ... & Zemp, M.: Heat stored in the Earth system 1960–2020: where does the energy go?. Earth System Science Data, 15(4), 1675-1709, 2023.

Wang, F., Shen, Y., Chen, Q., & Wang, W.: Bridging the gap between GRACE and GRACE follow-on monthly gravity field solutions using improved multichannel singular spectrum analysis. Journal of Hydrology, 594, 125972, 2021.

Wang, J., & Bras, R. L.: A model of evapotranspiration based on the theory of maximum entropy production. Water Resources Research, 47(3), 2011.

Wang, J., & Bras, R. L.: An extremum solution of the Monin–Obukhov similarity equations. Journal of the atmospheric sciences, 67(2), 485-499, 2010.

https://doi.org/10.5194/essd-2024-420
Preprint. Discussion started: 10 October 2024

Wang, J., Bras, R. L., Nieves, V., & Deng, Y.: A model of energy budgets over water, snow, and ice surfaces. Journal of Geophysical Research: Atmospheres, 119(10), 6034-6051, 2014.

Wang, K., & Dickinson, R. E.: A review of global terrestrial evapotranspiration: Observation, modeling, climatology, and climatic variability. Reviews of Geophysics, 50(2), 2012.

Wang, W., Chakraborty, T. C., Xiao, W., & Lee, X.: Ocean surface energy balance allows a constraint on the sensitivity of precipitation to global warming. Nature Communications, 12(1), 2115, 2021.

Wentz, F. J., Ricciardulli, L., Hilburn, K., & Mears, C.: How much more rain will global warming bring?. Science, 317(5835), 233-235. 2007.

Wielicki, B. A., B. R. Barkstrom, E. F. Harrison, R. B. Lee III, G. L. Smith, and J. E. Cooper.: Clouds and the Earth's Radiant Energy System (CERES): An Earth Observing System Experiment, Bull. Amer. Meteor. Soc., 77, 853-868, 1996.

Wielicki, B. A., Barkstrom, B. R., Harrison, E. F., Lee III, R. B., Smith, G. L., & Cooper, J. E.: Clouds and the Earth's Radiant Energy System (CERES): An earth observing system experiment. Bulletin of the American Meteorological Society, 77(5), 853-868, 1996.

Xu, T., Guo, Z., Xia, Y., Ferreira, V. G., Liu, S., Wang, K., ... & Zhao, C.: Evaluation of twelve evapotranspiration products from machine learning, remote sensing and land surface models over conterminous United States. Journal of Hydrology, 578, 124105, 2019.

Yang, Y., & Roderick, M. L.: Radiation, surface temperature and evaporation over wet surfaces. Quarterly Journal of the Royal Meteorological Society, 145(720), 1118–1129, 2019.

Yang, Y., Roderick, M. L., Guo, H., Miralles, D. G., Zhang, L., Fatichi, S., ... & Yang, D.: Evapotranspiration on a greening Earth. Nature Reviews Earth & Environment, 4(9), 626-641, 2023.

Yang, Y., Sun, H., Zhu, M., Wang, J., & Zhang, W.: An R package of maximum entropy production model to estimate 41 years of global evapotranspiration. Journal of Hydrology, 614, 128639, 2022.

Yin, Y., Wu, S., Chen, G., & Dai, E.: Attribution analyses of potential evapotranspiration changes in China since the 1960s. Theoretical and applied climatology, 101, 19-28, 2010.

Yu, L., X. Jin, and R. A. Weller.: Multidecade Global Flux Datasets from the Objectively Analyzed Air-sea Fluxes (OAFlux) Project: Latent and sensible heat fluxes, ocean evaporation, and related surface meteorological variables. Woods Hole Oceanograp, 2008.

Yu, L.: A global relationship between the ocean water cycle and near-surface salinity. Journal of Geophysical Research: Oceans, 116(C10), 2011.

Zeng, X., Zhao, M., & Dickinson, R. E.: Intercomparison of bulk aerodynamic algorithms for the computation of sea surface fluxes using TOGA COARE and TAO data. Journal of Climate, 11(10), 2628-2644, 1998.

Zhao, G., & Gao, H.: Estimating reservoir evaporation losses for the United States: Fusing remote sensing and modeling approaches. Remote Sensing of Environment, 226, 109-124, 2019.

Zhao, G., Gao, H., Naz, B. S., Kao, S. C., & Voisin, N.: Integrating a reservoir regulation scheme into a spatially distributed hydrological model. Advances in Water Resources, 98, 16-31, 2016.

https://doi.org/10.5194/essd-2024-420
Preprint. Discussion started: 10 October 2024

Open Access Earth System Science Data Discussions

Zhao, G., Li, Y., Zhou, L., & Gao, H.: Evaporative water loss of 1.42 million global lakes. Nature Communications, 13(1), 3686, 2022.